Universitatea
Transilvania
din Brașov

INTERDISCIPLINARY DOCTORAL SCHOOL

Faculty of Mechanical Engineering

Ing. Ștefania OLĂREANU (căs. URSACHE)

Research concerning to the modeling and testing of the hybrid composite materials structures

SUMMARY

Scientific supervisors:

Prof. dr. ing. Camelia CERBU

Prof. dr. ing. Anton HADĂR

BRAȘOV, 2024

Universitatea Transilvania din Brașov

Mr. (Mrs.).....

COMPOSITION

Doctoral Commission

Named by order of the Rector of the Transilvania University of Brasov

No..... from.....

PRESIDENT:	Conf. dr. ing. COSTIUC Liviu, Transilvania University of Brasov
SCIENTIFIC SUPERVISORS:	Prof. dr. ing. CERBU Camelia, Transilvania University of Brasov Prof. dr. ing. HADĂR Anton, National University of Science and Technology POLITEHNICA Bucharest
OFFICIAL REVIEWER:	Prof. dr. ing. NĂSTĂSESCU Vasile, Military Technical Academy „Ferdinand I" from Bucharest Prof. dr. ing. BORDEAȘU Ilare, "Politehnica" University from Timisoara Prof. dr. ing. BÂRSĂNESCU Paul-Doru, Technical University "Gheorghe Asachi" Iasi

Date, time and place of public defence of the thesis: **12.09.2024**, hour **09^{00}**, room **CP8.**

Any assessments or observations on the content of the work will be transmitted electronically in due time, to the address of the stefania.olareanu@unitbv.ro

At the same time, we invite you to take part in the public meeting for the defense of the doctoral thesis.

Thank you.

Universitatea Transilvania din Brașov

Contents

Foreword

The doctoral thesis entitled " Research concerning to the modeling and testing of the hybrid composite materials structures" addresses a highly relevant topic, related to research on the mechanical behavior of composite materials reinforced with hybrid carbon fiber and aramid fiber fabric and represents a challenging and fulfilling personal experience.

In particular, I want to express my sincere gratitude, appreciation and respect to my scientific coordinators, Prof. Dr. Eng. Camelia Cerbu and Prof. Dr. Eng. Anton Hadăr, first of all, for believing in me, but also for their unconditional support during the entire period of my activity as a doctoral student. Their patience and academic rigor have guided me throughout the development of this PhD thesis and constantly motivated me to push my limits and contributed to my development as a researcher.

I would like to thank the members of the scientific guiding committee, Prof. Dr. Eng. Călin Ioan Roșca, Prof. Dr. Eng. Vasile Ciofoaia, Prof. Dr. Eng. Horațiu Teodorescu-Drăghicescu, Ș.l. Dr. Eng. Guiman Maria Violeta and Prof. Dr. Eng. Baciu Florin (National University of Science and Technology POLITEHNICA Bucharest), for their constant guidance and constructive remarks regarding my research work. Furthermore, my sincere thanks to Prof. Dr. Eng. Mariana Domnica Stanciu for her observations and recommendations during the public meeting for the pre-defense of the doctoral thesis.

I would also like to express my sincere gratitude to the distinguished members of the committee of the public defense of this doctoral thesis, for their appreciation of the content of the paper and for the time dedicated to participating in the public defense meeting of this doctoral thesis.

I would like to thank to the following people for the technical support given in order to carry out the experimental research: Ș.l. Dr. Eng. Horia Alexandru Petrescu and Prof. Dr. Eng. Anton Hadăr (National University of Science and Technology POLITEHNICA Bucharest), Ș.l. Dr. Eng. Alexandru Manolescu (Research-Development Institute of the Transilvania University in Brașov).

I would like to thank also to Prof. Dr. Eng. Camelia Cerbu for her assistance in the manual manufacture of the samples used in this doctoral thesis, as well as for carrying out experimental tests.

Thank you also to all the university professors who supported and encouraged me.

Last but not least, I would like to thank from the bottom of my heart my husband, Cezar, and my daughter, Victoria, for their constant encouragement and moral support, motivating me in the most difficult moments.

1. INTRODUCTION

In the last decades in the top fields of industry, such as aerospace, medical, maritime and military, the replacement of classic materials (wood, steel, glass, etc.) with composite materials, for the manufacture of structures, equipment and products that require to meet increasingly high mechanical and financial requirements. The study of composite materials is a vast field of research that continues to challenge scientists around the world. The mechanical properties of composite materials must be continuously improved to meet the increasing requirements. This is necessary to produce material structures that guarantee strength, stiffness, thermal stability, and fatigue and impact resistance while maintaining a lower specific weight. To create such innovative structures out of composite materials, one must first have a thorough understanding of the mechanical characteristics of the component materials (fibers and matrices). This allows for an analysis of the chemical interactions between the two constituents and how they cooperate under mechanical stress.

Also, a number of factors related to these two components (fibers and matrix) influence the mechanical properties of composite materials, such as: shape, nature, size and orientation of the fiber, volume fraction of the fiber, type and nature of the matrix. In recent years, many researchers have also turned their attention to studying the mechanical properties of hybrid composite materials. The studies were mainly focused on combinations of carbon fibers and other preferred types of fibers, less brittle. Through hybridization, the aim is mainly to reduce the mass of the resulting composite material and improve the mechanical performance by combining two or more types of fibers in the same composite material structure, but also to reduce production costs, by using cheaper fibers in those areas of composite structures where the state of stress is not at a very high level. In the field of hybrid composite materials, the following sub-categories of composites can be included:

- sandwich type structures – between two layers of a certain material, called the faces of the sandwich, a layer of a different material, called the core, is placed;
- inter-layer hybrid structures - in the structure of the composite material there are different reinforcing materials in various layers;
- hybrid structures inside the layer - two or more types of fibers are used for reinforcement in the same layer and are distributed regularly or randomly;
- "fiber by fiber" hybrid structures - the fibers that make up the reinforcing material are combined in an arbitrary way, so that there are no concentrations of a certain type of fibers in the structure of the composite material.

Thus, for the design and manufacture of a hybrid composite structure, the knowledge of the mechanical properties of the reinforcing materials (fibers) and how they chemically interact with the matrix material, play a decisive role in the analysis of the reliability and durability of these hybrid composite materials.

In the research carried out within the present doctoral thesis, it was proposed to investigate the mechanical behavior under the action of static mechanical stresses (traction and bending by the three-point method) and dynamic mechanical stresses (Charpy impact test and low-velocity impact

by free fall) of structures made of intra-layer hybrid composite material reinforced with carbon fibers and Kevlar (aramid) fibers.

Chapter 2 presents the current state of research on hybrid composite materials, reinforced with carbon fibers and Kevlar fibers. Thus, a series of mechanical properties of Kevlar fibers and carbon fibers are presented for which there are studies published in the specialized literature, these representing basic indicators for the final destination in different applications, of the composite material reinforced with such fibers. It also describes the current state of research on structures made of hybrid composite materials, reinforced with both Kevlar and carbon fibers. At the same time, this chapter highlights the advantages and disadvantages of hybridizing the two types of fibers. It also presents applications of composite materials reinforced with carbon fibers and/or Kevlar fibers in order to strengthen structural elements (wooden or concrete beams, panels), published in various specialized scientific works.

Chapter 3 briefly presents the objectives and purpose of the doctoral thesis, describes the main objective of this thesis and what are the secondary objectives pursued within the thesis.

Chapter 4 presents some analytical calculation models used in the mechanics of composite materials, leading to the calculation relationships used for the equivalent elastic properties of the layered compound materials required in their plane and for those required at bending. The basic notions in the micromechanics and marcomechanics of composite materials are synthesized for the purpose of explaining the sizes used in the analytical calculation model in the final chapters of the thesis.

Chapter 5 describes the experimental research carried out by the author of this doctoral thesis in order to determine the main mechanical and elastic characteristics for the composite material reinforced with carbon-aramid hybrid fabric. The materials tested, the working methods (both theoretical and experimental), the characteristics for the hybrid reinforcing fabric and for the matrix, the shape and the dimensions of the specimens subjected to the experimental tests are described. The experimental methods used for the characterization of the composite material are: the tensile test combined with the non-invasive method of digital image correlation; bending test by the three-point method; impact test by the Charpy test. To determine the coefficient of transverse contraction in the plane of fiber reinforcement, the graphs of the variation of the specific contraction in the transverse direction of the specimen as a function of the specific elongation measured in the longitudinal direction are used. The mechanical properties obtained as a result of these tests are summarized in the tables. Considering the determined elastic characteristics, both the analytical calculation model and the numerical modeling are used to simulate the stress and strain states that develop in the tensile and compressive stresses, to obtain the equivalent elastic moduli for the layered composite material involved in the study.

Chapter 6 addresses the issues related to impact behavior of two types of plates made of carbon-aramid hybrid fabric-reinforced composite material. The first set of samples 70 mm x 70 mm plates, made of eight layers of carbon-aramid hybrid fabric reinforced composite material. The second set of samples fabricated as sandwich plates having the same dimensions, with both sides made of three layers of composite material reinforced with carbon-aramid hybrid fabric and with a rubber core. To study the effect that water absorption has on the impact properties, part of the specimens of the two sets were impact tested before immersion and the other specimens were tested after immersion in water until saturation. The results obtained in the low-velocity impact test are presented

comparatively both for the two types of composite materials tested and for those tested after immersion in relation to those tested before immersion.

Chapter 7 presents the numerical modeling and flexural testing of thin-walled rectangular cross-section beams made of carbon-aramid hybrid fabric-reinforced composite material. Finally, the results obtained are graphically represented and compared with the results achieved in numerical simulation with finite elements and the results of experimental tests performed by combining the mechanical test with the optical method of determining 3D deformations and displacements by the DIC method. The experimental results are used to validate the numerical model of the beam subjected to bending, for which the modeling of the material was made taking into consideration the elastic characteristics determined in chapter 5 of this thesis.

Chapter 8 highlights the most significant conclusions of the research presented, the importance of the results obtained and the personal and original contributions of the author of the doctoral thesis in the field of research relating to the mechanical behavior of composite materials reinforced with carbon fibres and aramid fibres. Finally, the future directions of research that could be approached in the future by the author of this thesis and by other specialists and engineers in the same field of research are presented.

2. CURRENT STATE OF RESEARCH ON KEVLAR FIBERS, CARBON FIBERS AND CARBON FIBER AND KEVLAR FIBER REINFORCED HYBRID COMPOSITE STRUCTURES

In recent years, significant progress has been made in the field of hybrid composite materials research, due in particular to the development of the main industrial branches, which produce or use structures or components made of composite materials, due to their low weight and very good mechanical performances, among which we can mention: civil and industrial construction, the automotive industry, the aerospace industry, aeronautics, etc. The main purpose is to show the potential of carbon composites, Kevlar composites and Kevlar–carbon hybrid composite materials in order to use them for structural applications in civil engineering, based on their advantages concerning their high strength, stiffness and impact properties. For this purpose, this chapter intends to provide a summary of the main properties of the carbon and Kevlar fibres and of their composite materials, which make them recommendable for improvements in the strength and stiffness of structural elements. At the end of the chapter, some applications are described regarding the use of composite materials reinforced with carbon fibers and/or Kevlar fibers for the reinforcement/consolidation of structural elements (wooden or concrete beams, panels).

2.1.Properties of Kevlar fibres

2.1.1. Mechanical properties of Kevlar fibres

In Table 2.1, the tensile properties of the most common types of Kevlar fibres are summarized, which can be found on the market.

Table 2.1. Tensile properties for different Kevlar fibres [1].

Fibre Name	Young's Modulus E (GPa)	Poisson's Coefficient ν_{12}	Tensile Strength σ_{max} (GPa)	Extension to Break (%)	Density (g/cm^3)	References
Kevlar29	70	0,37	2,9	4	1,44	
Kevlar49	135	0,36	2,9	2,8	1,45	
Kevlar100	60	-	2,9	3,9	1,44	
Kevlar119	55	-	3,1	4,4	1,44	[2-4]
Kevlar129	99	-	3,4	3,3	1,45	
Kevlar149	143	0,30	2,3	1,5	1,47	
KevlarKM2	85	0,24	3,8	4,5	1,44	

2.1.2. Thermal properties of Kevlar fibres

In Table 2.2, the reported values in the literature are shown for the characteristics regarding the thermal degradation of Kevlar fibres.

Table 2.2. Characteristics of thermal degradation of Kevlar fibres [1].

Fibre Name	Heating Rate (°C/ min)	Degradation Rate (%/ min.)		Temperature of Decomposition (°C)		Weight Reduction (until decomposition) (%)		References
		Air	Nitrogen	Air	Nitrogen	Air	Nitrogen	
Kevlar	variabil	8,2	3,5	521,0	546,0	8	6	[6]
Kevlar29	20	26,0	21	449,1	480,0	9	8	[7]
Kevlar49	20	27,0	22	451,0	474,7	9	8	[7]
Kevlar49	10	-	-	482,0	538,0	9	8	[5]
Kevlar129	20	28,0	23	437,1	464,2	8	7	[7]

Kevlar fibres subjected to high temperatures demonstrate a different behaviour in the axial and transverse directions, showing a very small negative coefficient of thermal expansion (CTE) in the longitudinal direction of the fibres and a positive CTE in the transverse plane (table 2.3).
These values of CTE are provided in Table 2.3 along with the values of CTE from the one other reference

Table 2.3. Coefficient of thermal expansion for Kevlar fibres [1].

Fibre Name	Temperature Range (°C)	Coefficient of Thermal Expansion ($x\ 10^{-6}\ °C^{-1}$)		References
		Longitudinal	Transversal	
Kevlar29	25-150	-4,0	-	[5]
Kevlar49	25-150	-4,0	-	[5]
Kevlar49	20-80	-5,7	66,3	[8]

2.1.3. Impact properties of Kevlar fibres

Kevlar fibres are known as materials with very good impact strength. Kevlar fibres absorb a large amount of strain energy on impact and, as a result, are used for the manufacturing of ballistic protection panels and military protective equipment (bullet-proof vests, helmets, tactical gloves). Friction between the filaments is considered one of the most important parameters for characterizing the ballistic performance of Kevlar fabrics. Friction between yarns (yarn-toyarn friction) is generally evaluated by yarn pull-out force and is associated with impact strength. For regular Kevlar fibres the following properties were determinated [9]:

- yarn pull-out force: 20,2 N
- impact energy absorption: 103,12 J.

2.1.4. Influence of water absorption on Kevlar fibres

For Kevlar29 fibres, the decrease in both the fibre strength and Young's modulus is smaller, although these absorbed more water [1].
Table 2.4 shows the effects of water absorption on both Young's modulus and the tensile strength for three types of Kevlar fibres (Kevlar29, Kevlar49 and Kevlar149).

Table 2.4. The influence of water absorption on the mechanical properties of Kevlar fibres [1].

Fibre Name	Mechanical properties in dried fibres		Mechanical properties at saturation		Water absorption at saturation	Reference
	Young's Modulus E (GPa)	Tensile Strength σ_{max} (GPa)	Young's Modulus E (GPa)	Tensile Strength σ_{max} (GPa)	(%)	
Kevlar29	70	2,9	64	2,48	5,3	
Kevlar49	135	2,9	69,8	1,81	4,3	[10]
Kevlar149	143	2,3	100,2	1,69	2,1	

2.1.5. Effects of ultraviolet (UV) light on Kevlar fibres

It is well known from the literature that Kevlar fibres are sensitive to UV light. Upon exposure, the yellow or gold Kevlar fibres turn firstly orange and then brown because of their degradation. Also, prolonged exposure to UV light can cause the loss of mechanical properties, depending on the wavelength, exposure time, radiation intensity and product geometry. In conclusion, if the material is thicker, it is more protected because the outer fibers form a protective barrier, covering the inner fibers in a bundle of filaments or fabric. Thus the resistance loss is reduced to a minimum [5].
Table 2.5 summarizes the data obtained for different types of Kevlar fibers after being exposed to UV light.

Table 2.5. Effect of UV (ultraviolet) light on tensile strength of Kevlar fibres [1].

Fibre Size (denier)*	UV Exposure (h)	Tensile Strength after Exposure (%)	Reference
1500	450	35	[5]
3000		55	
4500		65	

*denier – Property unique to the fibre industries used to describe the fineness (and, conversely, the cross-sectional area) of individual filaments, thread, yarn, etc. It is defined as the weight expressed in grams, for 9000 m of a single filament.

2.2. Properties of carbon fibres

2.2.1. Mechanical properties of carbon fibres

Compared with other synthetic fibres (glass, aramid, nylon fibres), carbon fibres have numerous advantages, including high stiffness, high tensile strength, light weight, high chemical resistance, high temperature stability and a low thermal expansion coefficient.
Table 2.6 presents a classification of carbon fibres according to their mechanical properties.

Table 2.6. Example of a classification of carbon fibres [1].

Fibre Type	Main Characteristic	Tensile Strength σ_{max} (GPa)	Young's Modulus E (GPa)	References
UHM	Ultra-high modulus	>2,5	>600	[13-18]
HM	High modulus	>2,5	350-600	
IM	Intermediate-modulus	>3,5	280-350	
HT	High tensile strength (or standard modulus)	>3	200-280	
SHT	Super-high tensile strength	>4,5	<200	

2.2.2. Thermal properties of carbon fibres

Carbon fibres combine high tensile strength and high modulus of elasticity with low weight. Furthermore, this high tensile strength is maintained up to extremely high temperatures [19]. A decrease of 21.94% of the tensile strength (decreasing from 5.47 GPa down to 4.27 GPa) was recorded by heating at temperatures above 400 ◦C (tabel 2.7) [21]. Simultaneously, above this temperature, a reduction in the fibre diameter of approximately 37% was recorded [20].
Table 2.7 shows the influence of temperature on the tensile strength of carbon fibres.

Table 2.7. Influence of high temperatures on the tensile strength of carbon fibres [1].

Carbon fibre type *	Temperature exposure °C	Tensile Strength σ_{max} (GPa)	References
UHM	Room temperature	5,47	[21]
UHM	350	5,20	
UHM	450	4,27	
HT	Room temperature	4,60	[22]
HT	2840	2,60	

* UHM – ultra high modulus, HT – high tensile strength.

Carbon fibres subjected to high temperatures exhibit very good properties in terms of thermal conductivity and thermal expansion. Small coefficient of thermal expansion of the carbon fibres, makes them to be used in fields where high measurement precision is required [13, 23-25].

Table 2.8. Coefficients of thermal expansion for carbon fibres [1].

Fibre Name	Temperature (K)	Coefficient of Thermal Expansion (10-6/K)		References
		Longitudinal	Transversal	
P 100	Room temperature	-0,1	7,0	
PANEX 33	350	1,0	5,0	[23]
HTA 5131	450	0,8	6,0	
K-1100	Room temperature	-1,45	-	
T 1000	Room temperature	-0,55	-	[25]
M40J	Room temperature	-0,83	-	

It can be seen that negative values of the coefficient of thermal expansion were reported for carbon fibres in the longitudinal direction. Conversely, the coefficients of thermal expansion in the transverse direction of the carbon fibres were positive and higher than those measured in the longitudinal direction.

2.2.3. Electrical conductivity of carbon fibres

Carbon fibres are good electrical conductors and have a much longer service life than the metal cables. The capability of carbon fibres for transmitting electrical power is closely related to the graphitization process at different temperatures [26], As the graphitization temperature increases, the electrical conductivity increases. Table 2.9 shows the values of electrical conductivity according to the graphitization temperatures [27].

Table 2.9. Electrical conductivity of PAN-based carbon fibres [1].

Graphitization Temperature (°C)	Electrical Conductivity (S/cm)	Reference
1000	5,32	
1800	51,01	[27]
2200	75,91	

2.3. Mechanical characteristics of kevlar–carbon hybrid composite materials

2.3.1. Tensile and bending mechanical properties of Kevlar–carbon hybrid composite materials

In table 2.10 [32] the mechanical characteristics for such Kevlar–carbon hybrid composite materials are illustrated.

Table 2.10. Mechanical characteristics of hybrid composite materials reinforced with carbon and Kevlar fibres [1, 32].

Composite Structure *	Fibre Content	Young's Modulus E (GPa)	Tensile Strength σ_{max} (GPa)	Flexural Strength σ_{max} (GPa)	Poisson's Coefficient ν_{12}	Shearing Modulus of Elasticity G_{12} (GPa)	References
2K/8C/2K	60.0 % vol.	-	1,25	1,15	-	-	[30]
3C/2K/2C/ 2K/3C	60.0 % vol.	-	-	0,954	-	-	[30]
8CK plain	-	11,34	-	-	0,09	1,49	[33]
8CK twill	45.0 % mas.	35,25	4,07	4,18	0,141	-	[31]
CKCKC	37.2 % mas.	-	2,0	0,43	-	-	[34]
KCKCK	20.2 % mas.	-	2,4	0,50	-	-	[34]
KKCKK	38.4 % mas.	-	2,6	0,60	-	-	[34]
CCKCC	42.0 % mas.	-	2,7	0,46	-	-	[34]

*, C—carbon fibres; K—Kevlar fibres; CKCKC—hybrid composite material with 5 layers; 8CK plain—composit ematerial reinforced with 8 layers of Kevlar–carbon plain hybrid fabric; 8CK twill—composite material reinforced with 8 layers of Kevlar–carbon twill hybrid fabric; 2K/8C/2K—composite hybrid material reinforced with 2 layers of Kevlar49 fibres, 8 layers of carbon HT fibres and 2 layers of Kevlar49 fibres; 3C/2K/2C/2K/3C—composite hybrid material reinforced with 3 layers of carbon HT fibres, 2 layers of Kevlar49 fibres, 2 layers of carbon HT fibres, 2 layers of Kevlar49 fibres and 3 layers of carbon HT.

It can be seen that the flexural strength is the highest for the composite material reinforced with hybrid Kevlar–carbon woven fabric (8CK twill), approximately 27% higher than the results obtained for the multi-layered hybrid composite materials (2K/8C/2K).
In the case of hybrid Kevlar–carbon composite materials reinforced with Kevlar–carbon hybrid woven fabric in the same layer, the high stiffness of the carbon fibres combined with the high tenacity of Kevlar fibres leads to composite materials with very good mechanical characteristics.

2.3.2. Proprietăți de impact ale structurilor realizate din materiale compozite hibride armate cu fibre de carbon și fibre de Kevlar

The researchers have focused on studying the advantages and disadvantages of hybridization of the carbon fibres and Kevlar fibres, in particular regarding the performances of such hybrid composite materials in impact tests. Both the carbon and Kevlar fibres have demonstrated high tensile strength. Additionally, the carbon fibres provide high stiffness while the Kevlar fibres assure high impact strength. Most researchers have focused on the comparative study of the behaviour of such hybrid

composite structures in impact tests by replacing layers reinforced with carbon fibres with layers reinforced with Kevlar fibres [35]. Table 2.11 [32] summarizes some of the values of the strain energy absorbed in low velocity impact tests, both for multi-layered hybrid composite materials and for composites reinforced either with carbon fibres or with Kevlar fibres

Table 2.11. Absorbed strain energy in low velocity impact tests for composite materials reinforced with carbon fibres and/or with Kevlar fibres [1, 32].

Composite structure*	Impact speed (m/s)	Absorbed strain energy (J)	Failure mode	Reference
K-K	4,5	2,8	Fully penetrated	[35]
C-C		2,4		
C-K		3,1		
K-C		3,1		

*#-# – two-layered composite material; C—carbon fabric; K—Kevlar fabric. All tested samples had the dimensions of 100 mm × 100 mm

The experimental results (table 2.11) show that the hybridization of the carbon and Kevlar fibres in the composite structure leads to a value of 3,1 J for the absorbed strain energy, which is 29,17% or 10,71% higher than for the composites reinforced either with just carbon fibres or just with Kevlar fibres,respectively.

2.3.3. Structural elements consolidation with composite materials reinforced with carbon or/and Kevlar fibres

Figure 2.3 shows 3D sketch views of different types of beam strengthening, in longitudinal and transverse directions, to meet the different needs of construction engineers. For example, by bonding composite materials to the lower surface of reinforced concrete beams, continuously or partially (Fig. 2.3a and Fig. 2.3b), the flexural strength of the beam is improved. In addition, the bonding of composite materials on the bottom and side surfaces of the beam (fig. 2.3c), leads to the increase of both the load-bearing capacity and the limitation of cracks on the surface of the beam. The type of arrangement shown in figure 2.3d is used in principle to strengthen concrete beams, by applying composite materials on the outside of the beam, in the same position where the reinforcement (steel bars, stirrups) was placed inside the concrete beam, which which leads to an increase in shear strength and bending strength of that beam..

Figure 2.3. Lay-ups of laminated composite materials on the longitudinal and transversal directions of the beam: (a) applied on the entire length; (b) partially and continuously applied on the beam length; (c) applied continuously on bottom and lateral faces; (d) partially and discontinuously applied on the beam length and faces [1].

Similar to reinforced concrete beams, the strengthening of the bottom face of wooden beams may also be performed with sheets made of carbon fibre-reinforced plastics (CFRP). Using bending tests, Torang and Desharma [42] investigated the influence of the bonding of the carbon fibre laminates to the lower surface of wooden beams on differentlengths of the beam span. The test results summarizing the maximum force recorded at failure are presented in table 2.13. Analysing the results shown in table 2.13, it can be seen that the maximum force value for the wooden beam with CFRP strengthening along its entire span is 48,3% higher than the value recorded for the regular wooden beam (without CFRP strengthening) having the same dimensions.

Table 2.13. Experimental results on wood beams subjected to flexural tests [1].

Beam structure	Beam size $b \times h$ (mm x mm)	Maximum force F_{max} (N)	Reference
Wooden beam without CFRP strengthening	75 x 100	35313,45	[42]
Wooden beam with CFRP strengthening along the entire span (L_R)*		52378,00	
Wooden beam with CFRP strengthening along ¾ of the span (L_R)*		48499,67	
Wooden beam with CFRP strengthening along 1/4 of the span (L_R)*		36864,77	

*L_R – span.

Recent studies have focused on investigating the effects of Kevlar fibre-reinforced composites on the strengthening of the structural elements. However, these are not considered suitable for applications involving high compressive and bending stresses, as Kevlar fibres are known to have a tendency to bend and ultimately fail under such test conditions [43, 44].

The experimental results obtained by other researchers [45] in flexural tests are summarized, in terms of the values of the breaking forces and in terms of the number of cracks developed in both the concrete beam and the beams strengthened with Kevlar layers. Comparative studies were conducted between concrete beams without strengthening and concrete beams that were strengthened on the bottom faces with Kevlar fabric. The dimensions of the cross section of the concrete beams were 200mmin height and 150mmin width, with a length of 1000 mm. The concrete beams were reinforced with 12mmdiameter steel bars in the longitudinal direction and with 8mm diameter stirrups in the transversal direction. Considering the data from table 2.14, an increase can be seen of

up to 37,7% in terms of the failure load for the reinforced concrete beams strengthened with two layers of Kevlar laminates at the bottom of the beam and an increase of up to 88,4% for the concrete beams strengthened with two layers of Kevlar fabric in a U shape.

Table 2.14. Experimental results for concrete beams subjected to flexural tests [1].

Concrete beam structure*	Failure force (kN)	Number of cracks	Maximum moment (kN·m)	Reference
Concrete beam without Kevlar layers	70,50	6	10,58	[45]
Concrete beam with 1 Kevlar-laminated layer at bottom	84,06	3	12,61	
Concrete beam with 2 Kevlar-laminated layers at bottom	97,07	2	14,22	
Concrete beam with 1 Kevlar-laminated layer in U shape	119,26	No visible cracks	17,89	
Concrete beam with 2 Kevlar-laminated layers in a U shape	132,86	No visible cracks	19,93	

It is also of interest to follow the impact response of reinforced concrete (B.A.) beams reinforced with composite materials. In this sense, impact tests were carried out on reinforced concrete beams, reinforced at the top, but also at the bottom, with layers of carbon fibers and Kevlar fibers. Two reinforced concrete beams reinforced at the top and bottom with a layer of Kevlar fiber reinforced composite material and two reinforced concrete beams reinforced at the top and bottom with a layer of composite material were prepared for impact testing carbon fiber reinforced composite, to observe the role of each of the materials in the performance of the structure (fig. 2.4). For both beam configurations, repetitive impact tests were performed using a metal cylinder dropped from different heights onto the top surface of the beam. The results of the impact tests showed that the composite materials significantly increased the resistance capacity of the reinforced concrete beams. In addition, the laminates reduced deformations and crack sizes. By comparing test results for Kevlar and carbon fiber reinforced laminate beams, it was concluded that this increase in strength depends on the type, thickness, mass and properties of the composite material. In the case of reinforced concrete beams, not reinforced with composite materials, after the appearance of cracks, they would fail, but in the case of those reinforced with composite materials, even if cracks appeared as a result of the impact, the beam did not fail, it even resisted further impacts . This advantage is due to the use of Kevlar and carbon fiber laminates, which limit crack opening and increase shear strength [46].

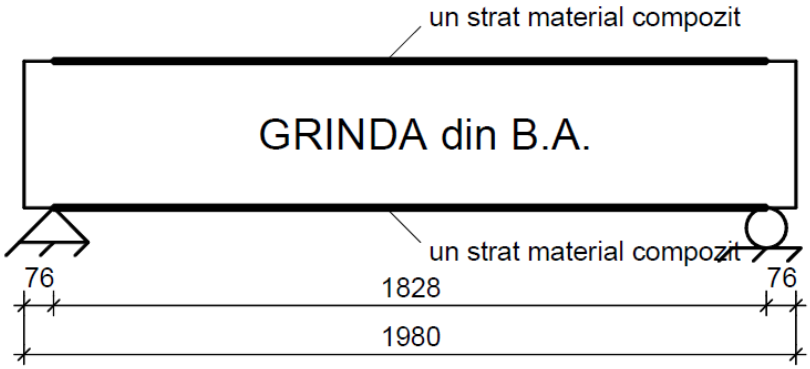

Figura 2.4. Concrete beam strenghtened with composite laminated layers [46].

In a recently published paper [47], impact tests were performed by free-falling a 12 kg mass from a height of 1,8 m onto the surface of wooden beams, reinforced and unreinforced at the bottom with composite materials reinforced with carbon fibers. During the impact tests, the beams were also subjected to an axial compressive force of 4 kN, to improve their impact resistance. Four types of samples were made to carry out the impact tests, as described in table 2.15. All four types of wooden beams tested had cross-sectional dimensions of 36 mm x 45 mm and their length was 360 mm. The results obtained from these impact tests are centralized in table 2.15.

Taking into account the experimental results obtained from the impact tests, it can be seen that the reinforcement at the bottom of the wooden beams with carbon fiber reinforced composite materials has a major influence on their impact resistance.

The results obtained in the impact tests showed that the reinforcement with a single layer of CFRP generates an increase in the impact strength of the wooden beam, but not so significantly, while the reinforcement with two layers of CFRP brings major improvements to the impact resistance of the beam from wood with an increase in impact energy by 182,17 % compared to the unreinforced wooden beam.

Table 2.15. Experimental results on wooden beams having the same dimensions, subjected to impact tests. [1].

Wood beam	Description	Impact strain energy absorbed (J)	Reference
G.L.	Wooden beam without CFRP strengthening	48,67	[47]
G.L.-1C	Wooden beam strengthened with 1 layer of CFRP	71,33	
G.L.-2C	Wooden beam strengthened with 2 layers of CFRP	137,33	
G.L.-11C	Wooden beam strengthened with 11 layers of CFRP	98,80	

2.4. Conclusion

After carrying out a critical analysis, in the specialized literature regarding the current state of research of hybrid composite materials reinforced with carbon fibers and with Kevlar fibers, the following conclusions can be formulated:

- the ever-increasing demand from the main industries for the manufacture of high-performance structures has led to a continuous development of the field of hybrid reinforced composite materials with carbon fibers and aramid fibers;
- a lack was identified regarding the experimental data related to the mechanical characteristics of hybrid composite materials reinforced with Kevlar fibers and carbon fibers, especially data related to Poisson's ratio and transverse elastic moduli;
- no information was identified regarding the structural strength elements, such as beams with a rectangular section made entirely of hybrid composite materials reinforced with Kevlar fibers and with carbon fibers;
- the hybrid structures studied are mainly of the interlayer type (in the structure of the composite material there are different reinforcing materials, in various layers), the research on the hybrid structures of the intra-layer type (two or more types of fibers are mixed in the same layer, in regularly or randomly) being relatively few;
- the perspective is to further develop solutions that allow obtaining structures from hybrid composite materials, with high performance, that ensure the reduction of costs and mass and are obtained through simple manufacturing technologies.

The main advantages and disadvantages regarding the hybridization of the two types of fibers (carbon fibers and aramid fibers or Kevlar) have been identified, namely:

a) Advantages of hybridizing Kevlar fibers and carbon fibers:

- materials with a very small thickness and low mass are obtained;
- composite materials characterized by high tensile strength, high rigidity due to carbon fiber reinforcement and high impact resistance due to Kevlar fiber reinforcement are obtained;
- composite materials are obtained with a low coefficient of thermal expansion compared to other hybrid materials, with high modulus of elasticity and high compressive strength;
- hybridization by increasing the content of carbon fibers leads to an increase in the strength or stiffness of the composite material, while by adding Kevlar fibers an increase in the flexibility of the composite materials is obtained;
- increasing the content of Kevlar fibers in the hybrid composite material increases impact resistance;

b) Disadvantages of hybridizing Kevlar fibers and carbon fibers:

- both carbon and Kevlar fibers have a high purchase cost;
- the lack of experimental data in the specialized literature regarding the elastic and resistance characteristics for these materials constitutes a disadvantage for the numerical simulation with finite elements of the structures made of such composite materials, mechanically stressed;
- by using Kevlar fibers for reinforcement of composite materials are obtained materials sensitive to the effects of humidity and to ultraviolet (UV) rays.

In this section, only a summary of the conclusions of the doctoral thesis is presented.

3. THE OBJECTIVES OF THE DOCTORAL THESIS

To establish the main objective of this doctoral thesis, the data synthesized in the previous chapter were taken into account, results from the study carried out on the current state of research on the mechanical properties of carbon fibers, aramid fibers (in particular, Kevlar) and composite materials reinforced with such fibers, as well as regarding their applications as structural elements (reinforcement of wooden or concrete beams, ballistic protection panels).
The main objective of the research carried out during the development of the doctoral thesis consists in the analysis of the mechanical behavior and in the determination of the mechanical properties under static (tension, bending) and dynamic (low-velocity impact) stresses for different structures made of composite materials reinforced with hybrid fabric (carbon fiber and aramid fiber). Considering the fact that aramid fibers, and implicitly Kevlar ones, are sensitive to umidity, which leads to the degradation of mechanical properties, it is necessary to consider the effect of water absorbtion on the mechanical behavior of the composite materials involved, which are reinforced with aramid fibers in addition to the fibers of carbon.

In order to achieve the main objective presented above, the following specific objectives were established for the doctoral thesis:

- critical analysis of specialized literature regarding the current state of research in the field of composite materials reinforced with carbon fibers, with aramid fibers or with both types of fibers, in order to identify the advantages and disadvantages of hybrid composite materials, as well as to establish the directions of research;
- fabricate plates made from hybrid composite materials, based on epoxy resin, reinforced with carbon-aramid hybrid fabric, followed by their cutting, to obtain specimens for mechanical tests (tensile, bending, Charpy impact test, low-velocity impact), according to the recommendations of international standards;
- the study of the analytical models used in the specialized literature for the calculation of mechanically stressed composite materials;
- carrying out experimental tests to determine the elastic and mechanical traction and bending characteristics, as well as the impact resistance for composite materials reinforced with carbon-aramid hybrid fabric;
- the numerical simulation of the states of tension and deformation that develop in the tensile and bending stresses of the specimens made of composite material reinforced with carbon-aramid hybrid fabric, as well as the validation of the numerical models with the data obtained from the experimental tests;
- the use of analytical models from the mechanics of composite materials for the calculation of the equivalent modulus of elasticity for the laminated carbo-aramid/epoxy composite

material, requested for traction and bending; comparing the results with those obtained experimentally and by numerical simulation;

- performing the low-velocity impact test for specimens made of layered composite materials, reinforced with carbon-aramid hybrid fabric, with and without a rubber core;
- the comparative analysis of the mechanical behavior in the low-velocity impact test of the specimens made of composite material, reinforced only with carbon-aramid fabric and of the sandwich type specimens, with faces made of the same composite material and with a rubber core;
- the study of water absorption up to saturation, for layered composite materials, reinforced with carbon-aramid hybrid fabric, with and without a rubber core;
- the study of the effects of water absorption on the impact behavior and on the absorbed energy for the two types of composite materials reinforced with carbon-aramid hybrid fabric, with and without a rubber core;
- design and fabricate beams from composite material reinforced with carbon-aramid hybrid fabric, having a rectangular section, with thin walls;
- the bending test of beams made of composite material reinforced with carbon-aramid hybrid fabric and the determination of deformation and displacement fields by the digital image correlation method;
- finite element numerical simulation of stress and strain states in the beam made of composite material reinforced with carbon-aramid hybrid fabric, subjected to bending;
- validation of the numerical model with finite elements of the beam made of composite material, reinforced with carbon-aramid hybrid fabric, subjected to bending, by comparison with the experimental results.

4. ASPECTS REGARDING ANALYTICAL CALCULATION MODELS IN THE MECHANICS OF COMPOSITE MATERIALS

4.1. Micromechanics of compsoite materials

Micromechanics of composite materials studies composite materials taking into account the interaction between the component materials, namely the fibers and the matrix.
The analysis at the micromechanical level is based on the following assumptions:

a. the material of the fibers is considered homogeneous and isotropic, having a linear elastic behavior until breaking;
b. the fibers are evenly distributed and perfectly aligned;
c. the material of the matrix is considered homogeneous and isotropic, having linear elastic behavior until breaking and with perfect adhesion to the fibers;
d. the fiber-reinforced layer is considered homogeneous at the macroscopic level, linearly elastic, orthotropic and without initial internal stresses.

Taking into account the assumptions described above, it is considered that both the fibers and the matrix are characterized by three elastic characteristics, and after combining these two materials, an anisotropic material will result, which is considered homogeneous at the macroscopic level. The unidirectional fiber reinforced composite material is an orthotropic material, to which nine elastic characteristics correspond to the axes 1, 2, 3 of the local coordinate system (axis 1 is parallel to the direction of the fibers, axis 2 is perpendicular to the fibers, and axis 3 perpendicular to the first two axes):
E_1 – modulus of elasticity in the direction of the fibers;
E_2 – modulus of elasticity in the direction perpendicular to the fibers;
G_{12} – the transverse modulus of elasticity in the plane of fiber reinforcement;
G_{13} și G_{23} – the transverse interlaminar elastic moduli in plane 13 and in plane 23, respectively;
ν_{12} – Poisson's ratio in the plane of fiber reinforcement;
$\nu_{21} = \nu_{12}$ – Poisson's ratio in the secondary plane;
ν_{13} și ν_{23} – Poisson's ratio in planes 13 and 23, respectively.

The elastic and mechanical characteristics of the composite material can be estimated through analytical calculation models, based on the rule of mixtures, starting from the characteristics of each of the constituents.
For a composite material, the following sizes are defined:
i. the volume ratio of the fibers, as the ratio between the volume of the contained fibers and the total volume of the composite material;
ii. the volume ratio of the matrix, as the ratio between the volume of the matrix and the total volume of the composite material;
iii. the mass percentage of the fibers, as the ratio between the mass of the fibers and the total mass of the composite material;

iv. the mass percentage of the matrix, as the ratio between the mass of the matrix and the total mass of the composite material.

Taking into account the above, it follows that the sum of the two volume ratios is equal to unity [49-51]:

$$V_f + V_m = 1. \tag{4.1}$$

Analogously, since the total mass of the composite is given by the sum of the mass of the matrix and the mass of the fiber, it follows that [49-51]:

$$M_f + M_m = 1. \tag{4.2}$$

With the help of previously defined sizes and knowing the modulus of elasticity E_f, of the fibers as well as the modulus of elasticity E_m of the matrix, the calculation relations for the following elastic characteristics of unidirectional fiber reinforced composite material can be demonstrated [50]:

- the modulus of elasticity in the direction of the fibers and in the direction perpendicular to the fibers, denoted by E_1 and respectively, with E_2:

$$E_1 = E_f V_f + E_m V_m; \tag{4.3}$$

$$E_2 = \frac{E_f E_m}{E_f V_m + E_m V_f}; \tag{4.4}$$

- Poissons's ratio ν_{12}:

$$\nu_{12} = \nu_f V_f + \nu_m V_m; \tag{4.5}$$

- the transverse modulus of elasticity in the plane of fiber reinforcement G_{12}:

$$G_{12} = \frac{G_f G_m}{G_f V_m + G_m V_f}; \tag{4.6}$$

Based on the assumptions that the fibers and the matrix are considered homogeneous, isotropic materials with a linear elastic behavior, the relationships between their elastic characteristics are defined as follows:

$$G_f = \frac{E_f}{2(1+\nu_f)}; \qquad G_m = \frac{E_m}{2(1+\nu_m)}. \tag{4.7}$$

4.2. Mechanics of the composite layer

Two coordinate systems are used in the design and calculation models of structures made of composite materials:

- the local cartesian coordinate system (layer coordinate system), whose axes are denoted by 1, 2 and 3. Axis 1 is in the direction of the fibers, axis 2 is in the reinforcement plane and is perpendicular to axis 1, and axis 3 is perpendicular to the plane formed by axes 1 and 2 and to the surface of the composite material shell. Each layer has its own local coordinate system, and for each, axis 1 is parallel to the fiber direction (fig. 4.1.).
- the global coordinate system, whose axes are denoted by x, y, and z and to which all layers of the composite material are related.

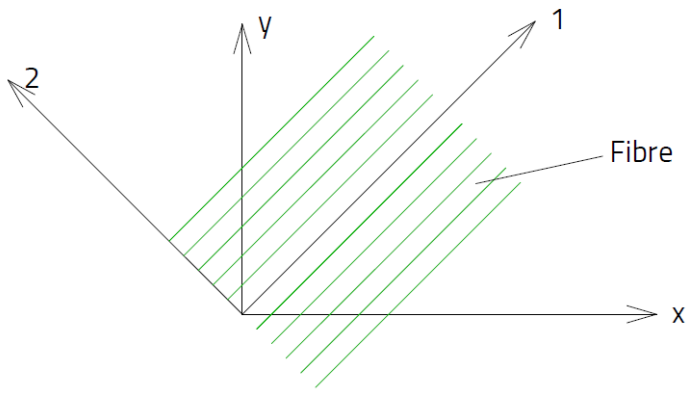

Figura 4.1. Local cartesian coordinate system and global coordinate system.

The stress state at each point of the composite material is characterized by the stress tensor. With respect to the local coordinate system of the layer, the stress tensor is expressed by the relation [49-52]:

$$[\sigma] = \begin{bmatrix} \sigma_1 & \tau_{12} & \tau_{13} \\ \tau_{12} & \sigma_2 & \tau_{23} \\ \tau_{13} & \tau_{23} & \sigma_3 \end{bmatrix}. \tag{4.8}$$

The stress tensor in relation to the global coordinate system is written in the form:

$$[\sigma] = \begin{bmatrix} \sigma_x & \tau_{xy} & \tau_{xz} \\ \tau_{yx} & \sigma_y & \tau_{yz} \\ \tau_{zx} & \tau_{zy} & \sigma_z \end{bmatrix}. \tag{4.9}$$

According to the law of duality of tangential stresses (Cauchy's law), the stress tensor is known to be symmetric, since [52, 53]:

$$\tau_{ij} = \tau_{ji}. \tag{4.10}$$

The strain tensor is symmetric and is written in the following forms [52-56], relative to the material coordinate system and, respectively, relative to the global coordinate system:

$$[\varepsilon] = \begin{bmatrix} \varepsilon_1 & \frac{\gamma_{12}}{2} & \frac{\gamma_{13}}{2} \\ \frac{\gamma_{12}}{2} & \varepsilon_2 & \frac{\gamma_{23}}{2} \\ \frac{\gamma_{13}}{2} & \frac{\gamma_{23}}{2} & \varepsilon_3 \end{bmatrix}; \tag{4.11}$$

$$[\varepsilon] = \begin{bmatrix} \varepsilon_x & \frac{\gamma_{xy}}{2} & \frac{\gamma_{xz}}{2} \\ \frac{\gamma_{xy}}{2} & \varepsilon_y & \frac{\gamma_{yz}}{2} \\ \frac{\gamma_{xz}}{2} & \frac{\gamma_{yz}}{2} & \varepsilon_z \end{bmatrix}. \tag{4.12}$$

In the plane stress state, the relationships between stresses and strains can be expressed taking into account the mechanical characteristics of the laminate, relative to the local coordinate system, as follows:

- the total value of the specific normal deformation in direction 1 of the fibers is given by the relation [55, 56]:

$$\varepsilon_1 = \frac{\sigma_1}{E_1} - \frac{\sigma_2}{E_2} \nu_{21}; \tag{4.13}$$

- the total value of the specific deformation for direction 2 perpendicular to the fibers, is given by the relation [47, 54, 55]:

$$\varepsilon_2 = -\frac{\nu_{12}}{E_1} \sigma_1 + \frac{\sigma_2}{E_2}. \tag{4.14}$$

Hooke's law being accepted, the tangential stresses are given by the following relations [50, 53, 54]:

$$\tau_{12} = G_{12} \cdot \gamma_{12} \tag{4.15}$$

$$\tau_{23} = G_{23} \cdot \gamma_{23} \tag{4.16}$$

$$\tau_{13} = G_{13} \cdot \gamma_{13} \tag{4.17}$$

In the case of composite materials, as a rule, the modulus of elasticity transverse to planes 12 and 13 do not differ much and therefore it can be approximated in the calculations that $G_{12} \cong G_{13}$.

Taking into account the mentioned, the strain-stress relations in relation to the local coordinate system of the layer, are written in the following form, for the thin layer of composite material [48, 51, 55, 56-58]:

$$\begin{Bmatrix}\varepsilon_1\\ \varepsilon_2\\ \gamma_{12}\end{Bmatrix}=\begin{bmatrix}\frac{1}{E_1} & -\frac{\nu_{12}}{E_1} & 0\\ -\frac{\nu_{12}}{E_1} & \frac{1}{E_2} & 0\\ 0 & 0 & \frac{1}{G_{12}}\end{bmatrix}\begin{Bmatrix}\sigma_1\\ \sigma_2\\ \tau_{12}\end{Bmatrix}=[S]\{\sigma\} \tag{4.18}$$

și

$$\begin{Bmatrix}\gamma_{23}\\ \gamma_{13}\end{Bmatrix}=\begin{bmatrix}\frac{1}{G_{23}} & 0\\ 0 & \frac{1}{G_{13}}\end{bmatrix}\begin{Bmatrix}\tau_{23}\\ \tau_{13}\end{Bmatrix}=[S^*]\{\tau\}, \tag{4.19}$$

$\{\varepsilon\}=\{\varepsilon_1 \quad \varepsilon_2 \quad \gamma_{12}\}^T$ is the strain vector in the reinforcement plane; $\{\sigma\}=\{\sigma_1 \quad \sigma_2 \quad \tau_{12}\}^T$ is the stress vector in the reinforcement plane; $\{\tau\}=\{\tau_{23} \quad \tau_{13}\}^T$ is the interlaminar stress vector; $[S]$ este the inverse of the reduced generalized elasticity modulus matrix $[Q]$; $[S^*]$ represents the inverse of the interlaminar modulus of elasticity matrix $[Q^*]$.

After inverting the matrix $[S]$, the relationship between the stress vector and the strain vector, in the plane of fiber reinforcement, can be written as [48, 50, 51, 56-58]:

$$\begin{Bmatrix}\sigma_1\\ \sigma_2\\ \tau_{12}\end{Bmatrix}=\begin{bmatrix}\frac{E_1}{\Delta} & \frac{\nu_{12}E_2}{\Delta} & 0\\ \frac{\nu_{12}E_2}{\Delta} & \frac{E_2}{\Delta} & 0\\ 0 & 0 & G_{12}\end{bmatrix}\begin{Bmatrix}\varepsilon_1\\ \varepsilon_2\\ \gamma_{12}\end{Bmatrix}=[Q]\{\varepsilon\}, \tag{4.20}$$

unde $\Delta= 1-\nu_{12}\nu_{21}=1-\nu_{12}^2E_2/E_1$.

Also, the relationship between the vector of interlaminar tangential stresses and the vector of specific interlaminar slips is [50, 55, 56]:

$$\begin{Bmatrix}\tau_{23}\\ \tau_{13}\end{Bmatrix}=\begin{bmatrix}G_{23} & 0\\ 0 & G_{13}\end{bmatrix}\begin{Bmatrix}\gamma_{23}\\ \gamma_{13}\end{Bmatrix}=[Q^*]\{\gamma\}. \tag{4.21}$$

The terms of the reduced generalized elasticity modulus matrix $[Q]$ [50]:

$$\begin{aligned} Q_{11}&=\frac{E_1}{\Delta}; & Q_{66}&=G_{12};\\ Q_{12}&=Q_{21}=\frac{\nu_{12}E_2}{\Delta}; & Q_{44}^*&=G_{23};\\ Q_{22}&=\frac{E_2}{\Delta}; & Q_{55}^*&=G_{13}\,. \end{aligned} \tag{4.22}$$

The relationship between the stress vector and the strain vector relative to the global coordinate system is defined by [50]:

$$\begin{Bmatrix}\sigma_x\\ \sigma_y\\ \tau_{xy}\end{Bmatrix}=\begin{bmatrix}\overline{Q}_{11} & \overline{Q}_{12} & \overline{Q}_{16}\\ \overline{Q}_{12} & \overline{Q}_{22} & \overline{Q}_{26}\\ \overline{Q}_{16} & \overline{Q}_{26} & \overline{Q}_{66}\end{bmatrix}\begin{Bmatrix}\varepsilon_x\\ \varepsilon_y\\ \gamma_{xy}\end{Bmatrix}=[\overline{Q}]\begin{Bmatrix}\varepsilon_x\\ \varepsilon_y\\ \gamma_{xy}\end{Bmatrix}, \tag{4.23}$$

$\overline{Q}_{ij}$ are the terms of the transformed reduced generalized elasticity modulus matrix.

In the same way, the following relation can be written for the tangential stresses [50]:

$$\begin{Bmatrix}\tau_{yz}\\ \tau_{xz}\end{Bmatrix}=\begin{bmatrix}\overline{Q}^{*}_{44} & \overline{Q}^{*}_{45}\\ \overline{Q}^{*}_{45} & \overline{Q}^{*}_{55}\end{bmatrix}\begin{Bmatrix}\gamma_{yz}\\ \gamma_{xz}\end{Bmatrix}, \tag{4.24}$$

$\left[\overline{Q}^{*}\right]$ is the transformed interlaminar modulus matrix.

4.3. Macromechanics of composite plate element

Starting from the assumptions presented, the constitutive equation of a layered composite plate element is described by the relationship below [50]:

$$\begin{Bmatrix}N_x\\ N_y\\ N_{xy}\\ M_x\\ M_y\\ M_{xy}\end{Bmatrix}=\begin{bmatrix}A_{11}A_{12}A_{16}B_{11}B_{12}B_{16}\\ A_{12}A_{22}A_{26}B_{12}B_{22}B_{26}\\ A_{16}A_{26}A_{66}B_{16}B_{26}B_{66}\\ B_{11}B_{12}B_{16}D_{11}D_{12}D_{16}\\ B_{12}B_{22}B_{26}D_{12}D_{22}D_{26}\\ B_{16}B_{26}B_{66}D_{16}D_{26}D_{66}\end{bmatrix}\begin{Bmatrix}\varepsilon_x^0\\ \varepsilon_y^0\\ \gamma_{xy}^0\\ \kappa_x\\ \kappa_y\\ \kappa_{xy}\end{Bmatrix}; \tag{4.25}$$

$$\begin{Bmatrix}T_y\\ T_x\end{Bmatrix}=\begin{bmatrix}H_{44} & H_{45}\\ H_{45} & H_{55}\end{bmatrix}\begin{Bmatrix}\gamma_{yz}\\ \gamma_{xz}\end{Bmatrix},$$

$N_x, N_y,$ are the axial forces, N_{xy} is the shear force per unit length along the boundary of the volume element in the composite plate; T_x, T_y are the shear forces per unit length of the plate; M_x, M_y sunt momentele de încovoiere, M_{xy} is the moment of torsion per unit length of the plate; $\varepsilon_x^0, \varepsilon_y^0, \gamma_{xy}^0$ are the deformations in the median surface; $\kappa_x^0, \kappa_y^0, \kappa_{xy}^0$ are the curvatures of the plate caused by bending and torsion; terms A_{ij} are part of the in-plane stiffness matrix $[A]$; terms B_{ij} are part of the bending stiffness matrix $[B]$; terms D_{ij} are part of the bending stiffness matrix $[D]$; terms H_{ij} are part of the transverse shear stiffness matrix $[H]$.

The relationship between the sectional forces developed at the level of the median surface of the plate element made of composite material and displacements and, respectively, curvatures, is defined by the constitutive equation [50, 52]:

$$\{N_x \quad N_y \quad N_z \quad M_x \quad M_y \quad M_z\}^T=\begin{bmatrix}[A] & [B]\\ [B] & [D]\end{bmatrix}\{\varepsilon_x^0 \quad \varepsilon_y^0 \quad \gamma_{xy}^0 \quad \kappa_x^0 \quad \kappa_y^0 \quad \kappa_{xy}^0\}^T. \tag{4.26}$$

Matrices terms $[A]$, $[B]$, $[D]$ are calculated with the following relations [50, 51]:

$$\begin{cases} A_{ij} = \sum_{k=1}^{n} \left(\bar{Q}_{ij}\right)_k (z_k - z_{k-1}) = \sum_{k=1}^{n} \left(\bar{Q}_{ij}\right)_k t_k; \quad D_{ij} = \frac{1}{3}\sum_{k=1}^{n} \left(\bar{Q}_{ij}\right)_k \left(z_k^3 - z_{k-1}^3\right). \\ B_{ij} = \frac{1}{2}\sum_{k=1}^{n} \left(\bar{Q}_{ij}\right)_k \left(z_k^2 - z_{k-1}^2\right); \end{cases} \quad (4.27)$$

t_k is the layer thickness k; z_{k-1} and z_k are the k-layer coordinates relative to the mid-plate surface.

Using equation (4.26) we get equation (4.28), which relates strains, bends and sectional stresses [49, 50, 55, 56]:

$$\{\varepsilon_x^0 \quad \varepsilon_y^0 \quad \varepsilon_z^0 \quad \kappa_x^0 \quad \kappa_y^0 \quad \kappa_{xy}^0\}^T = \begin{bmatrix} [\alpha] & [\beta] \\ [\beta] & [\delta] \end{bmatrix} \{N_x \quad N_y \quad N_z \quad M_x \quad M_y \quad M_z\}^T. \quad (4.28)$$

4.4. The analytical calculation model for layered composite materials, required in the reinforcement plan

To determine the mechanical characteristics of this layered, orthotropic and symmetric composite material, it is assumed that the in-plane stresses $(\sigma_x, \sigma_y, \tau_{xy})$ are uniformly distributed over the thickness of the plate in the case of plane loading, and the strain vector relative to the median surface of the orthotropic plate is calculated with equation (4.29), depending on the elastic properties of the orthotropic material and the stress vector [50, 57]:

$$\begin{Bmatrix} \varepsilon_x^0 \\ \varepsilon_y^0 \\ \gamma_{xy}^0 \end{Bmatrix} = \begin{bmatrix} 1/E_x & -\nu_{xy}/E_x & 0 \\ -\nu_{xy}/E_x & 1/E_y & 0 \\ 0 & 0 & 1/G_{xy} \end{bmatrix} \begin{Bmatrix} \sigma_x \\ \sigma_y \\ \tau_{xy} \end{Bmatrix} = \begin{bmatrix} 1/E_x & -\nu_{xy}/E_x & 0 \\ -\nu_{xy}/E_x & 1/E_y & 0 \\ 0 & 0 & 1/G_{xy} \end{bmatrix} \frac{1}{t} \begin{Bmatrix} N_x \\ N_y \\ N_{xy} \end{Bmatrix}. \quad (4.31)$$

Equating the terms of equation (4.29) and (4.31), the equivalent elastic properties $(E_x, E_y, G_{xy}, \nu_{xy})$ of the symmetric and orthotropic layer, required by forces acting in the plane of the reinforcement, can be determined with the relations below [50, 51]:

$$\begin{cases} E_x = 1/(t\alpha_{11}) = (A_{11}A_{22} - A_{12}^2)/(tA_{22}); \quad G_{xy} = 1/(t\alpha_{66}) = A_{66}/t; \\ E_y = 1/(t\alpha_{22}) = (A_{11}A_{22} - A_{12}^2)/(tA_{11}); \quad \nu_{xy} = -t\alpha_{12}E_x = -\alpha_{12}/\alpha_{11} = A_{12}/A_{22}. \end{cases} \quad (4.32)$$

4.5. The analytical calculation model for layered composite materials, stressed in bending

Since no force develops in the reinforcement plane, the strain vector corresponding to the point in the median surface is a null vector, according to equation (4.29). Thus, the vector of deformations at any

point in the layer, located at the distance z from the median surface, is calculated with the following relation [50]:

$$\{\varepsilon_x \quad \varepsilon_y \quad \gamma_{xy}\}^T = \{\varepsilon_x^0 \quad \varepsilon_y^0 \quad \gamma_{xy}^0\}^T + z\{\kappa_x^0 \quad \kappa_y^0 \quad \kappa_{xy}^0\}^T = z\{\kappa_x^0 \quad \kappa_y^0 \quad \kappa_{xy}^0\}^T. \tag{4.33}$$

Considering the relationship between the vector of moments and the vector of stresses corresponding to the stress components developed in the xy plane of the fictitious orthotropic plate and then, substituting the relations between stresses and strains, we obtain the equation [50]:

$$\begin{Bmatrix} M_x \\ M_y \\ M_{xy} \end{Bmatrix} = \int_{-t/2}^{t/2} \begin{Bmatrix} \sigma_x \\ \sigma_y \\ \tau_{xy} \end{Bmatrix} z\mathrm{d}z = \int_{-t/2}^{t/2} \begin{bmatrix} 1/E'_x & -\nu_{xy}/E'_x & 0 \\ -\nu_{xy}/E'_x & 1/E'_y & 0 \\ 0 & 0 & 1/G'_{xy} \end{bmatrix}^{-1} \begin{Bmatrix} \varepsilon_x \\ \varepsilon_y \\ \gamma_{xy} \end{Bmatrix} z\mathrm{d}z \tag{4.34}$$

Substituting in equation (4.34) the expression of the strain vector from equation (4.33), the following equation is obtained [50]:

$$\begin{aligned} \begin{Bmatrix} M_x \\ M_y \\ M_{xy} \end{Bmatrix} &= \begin{bmatrix} 1/E'_x & -\nu_{xy}/E'_x & 0 \\ -\nu_{xy}/E'_x & 1/E'_y & 0 \\ 0 & 0 & 1/G'_{xy} \end{bmatrix}^{-1} \begin{Bmatrix} \kappa_x^0 \\ \kappa_y^0 \\ \kappa_{xy}^0 \end{Bmatrix} \int_{-t/2}^{t/2} z^2\mathrm{d}z \\ &= \frac{t^3}{12} \begin{bmatrix} 1/E'_x & -\nu_{xy}/E'_x & 0 \\ -\nu_{xy}/E'_x & 1/E'_y & 0 \\ 0 & 0 & 1/G'_{xy} \end{bmatrix}^{-1} \begin{Bmatrix} \kappa_x^0 \\ \kappa_y^0 \\ \kappa_{xy}^0 \end{Bmatrix}. \end{aligned} \tag{4.35}$$

Using equation (4.35), the vector of curves $\{\kappa_x^0 \quad \kappa_y^0 \quad \kappa_{xy}^0\}^T$, written in terms of the vector of moments, is of the form [50]:

$$\begin{Bmatrix} \kappa_x^0 \\ \kappa_y^0 \\ \kappa_{xy}^0 \end{Bmatrix} = \frac{12}{t^3} \begin{bmatrix} 1/E'_x & -\nu_{xy}/E'_x & 0 \\ -\nu_{xy}/E'_x & 1/E'_y & 0 \\ 0 & 0 & 1/G'_{xy} \end{bmatrix} \begin{Bmatrix} M_x \\ M_y \\ M_{xy} \end{Bmatrix}. \tag{4.36}$$

Comparing equation (4.30) with equation (4.36), the equivalent elastic characteristics $(E'_x, E'_y, G'_{xy}, \nu'_{xy})$ for layered composite material, especially orthotropic, symmetrical, loaded only by bending moments $(M_{x,}, M_y)$ and the torque M_{xy}, is calculated using the following two relations [50]:

$$\begin{cases} E'_x = 12/(t^3\delta_{11}) = 12(D_{11}D_{22} - D_{12}^2)/(t^3 D_{22}); & G'_{xy} = 12/(t^3\delta_{66}) = 12\,D_{66}/t^3; \\ E'_y = 12/(t^3\delta_{22}) = 12(D_{11}D_{22} - D_{12}^2)/(t^3 D_{11}); & \nu'_{xy} = -t^3\delta_{12}E_x/12 = -\dfrac{\delta_{12}}{\delta_{11}} = \dfrac{D_{12}}{D_{22}}. \end{cases} \tag{4.37}$$

4.6. Concluzii

The calculation models presented in this chapter are used to calculate the elastic and mechanical characteristics corresponding to a layer of a composite material. Bearing in mind that the layers of a composite material are made up of reinforcing material (fibres) and matrix (usually resin) in different proportions, the properties of composite materials depend on: the nature of the fibres, their proportion to the matrix and the type of matrix . The transformation relations from the material coordinate system (having axes 1, 2, 3) to the Oxyz global coordinate system and vice versa are presented. If the elastic and mechanical properties of the composite material are known during the design phase of a part made of such material, its shape and geometry can be optimized so that, in the end, it meets the mechanical demands for which it was designed, both in terms of stiffness and strength. The presented analytical calculation models are based on equating the layered composite material with a fictitious orthotropic material, which has the same mechanical behavior.
In this section, only a summary of the conclusions of the doctoral thesis is presented.

5. DETERMINATION OF MECHANICAL AND ELASTIC CHARACTERISTICS FOR COMPOSITE MATERIAL REINFORCED WITH CARBON FIBER AND ARAMID FIBER HYBRID FABRIC

5.1. Materials tested

Carbon-aramid woven fabric of type SIGRATEX H W215-TW2/2 manufactured by SGL Carbon (Wiesbaden, Germany), was used to reinforce the Epolam 2031 complex of epoxy resin and its corresponding hardener (manufactured by Axson Technologies, USA). SIGRATEX H W215-TW2/2 carbon-aramid woven fabric whose density is 215 g/m^2, is a bidirectional twill hybrid fabric containing the both kinds of fibres, carbon fibres and aramid fibres, on both directions (fig. 5.1).

Figure 5.1. Photo of the SIGRATEX H W215-TW2/2 twill woven carbon-aramid fabric used to reinforce the laminated composite material tested [60].

Epoxy resin of type Epolam 2031 is mixed with Epolam 2031 hardener before impregnation of the carbon-aramid woven fabric, the mix ratio by volume being equal to 100:33 according to datasheet of the resin [61]. The composite panel whose dimensions were 600 mm x 460 mm, was made of eight layers reinforced with SIGRATEX H W215-TW2/2 twill carbon-aramid fabric. The fibre weight ratio was equal to 45 wt. %. The thickness of the composite panel was approximately equal with 2.6 mm. It has to be noted that the orientation of the reinforcement carbon-aramid fabric was kept the same in all layers of the composite. Two sets of specimens corresponding to the warp and weft directions of the reinforcement carbon-aramid woven fabric, were cut for each type of mechanical test involved: tensile test, bending test by three's point method; impact test by Charpy method.

5.2. Experimental work method

5.2.1. Tensile test

Universal testing machine LFV50-HM, 980 (Walter&Bai, Switzerland) whose maximum force is 200 kN was used in tensile test. This machine has digital control and the following data may be recorded by its controlling software installed on computer: tensile force F, elongation Δl of the tensile specimen and time t. The aim of the tensile test is to determine the following properties of the composite material involved in this research: tensile modulus of elasticity, tensile strength, Poisson's ration (transverse contraction coefficient). For this purpose, the tensile test was combined with DIC

method in order to use virtual extensometers for determination of real elongation and strains of the specimens. By the DIC method, the extensometer or strain gauges as measurement instruments are replaced with some virtual ones without additional costs of consumable materials. This is just one of the advantages of the DIC method.

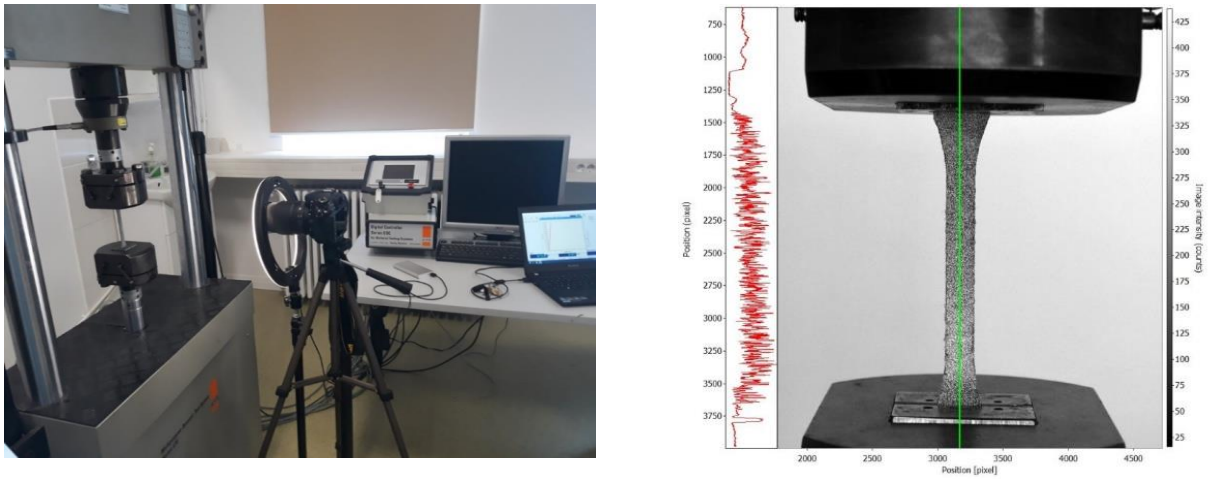

(a) (b)

Figure 5.2. Experimental setup in tensile test combined with DIC method: (a) configuration of the test; (b) speckle image of the tensile specimen [31].

5.2.2. Bending test

Universal testing machine manufactured by Walter&Bai (Switzerland) whose maximum force is 100 kN was used in bending test (building L9 from the Research and Development Institute of Transilvania University in Brașov). It is determined the average flexural modulus of elasticity and the average flexural strength for each set of specimens corresponding to the both warp and weft directions of the reinforcement carbon-aramid woven fabric. The flexural modulus of elasticity E' is computed by using the initial linear portion of the curves which plot the variation of the bending force in function of the deflection v.

$$E' = \frac{l^3}{48 I_z} \cdot \frac{\Delta F}{\Delta v} \tag{5.1}$$

where l is the span of the flexural specimen between the simple supports; I_z represents the axial moment of inertia of the cross section of the specimen with respect to the neutral axis.

5.2.3. Charpy impact test

For Charpy impact test it was used the pendulum impact tester HIT50P manufactured by Zwick/Roell (Ulm, Germany). The specimen is simply supported at both ends and the impact hammer strikes the middle of the specimen in the Charpy impact test. The pendulum impact tester HIT50P with digital controlling measures and displays the failure energy W for each specimen tested. The impact

strength *K* or resilience corresponding to each specimen is computed as the ratio between the failure energy *W* and the area *A* of the specimen cross-section by using Equation:

$$K = U/A. \tag{5.2}$$

5.3. Finite element analysis

5.3.1. Simulation of the tensile test of the specimen made of laminated composite material reinforced with carbon-aramaid hybrid fabric

The numerical simulation of the tensile test of the specimen made of laminated composite material involved in this research was used by using the software Abaqus, student version.

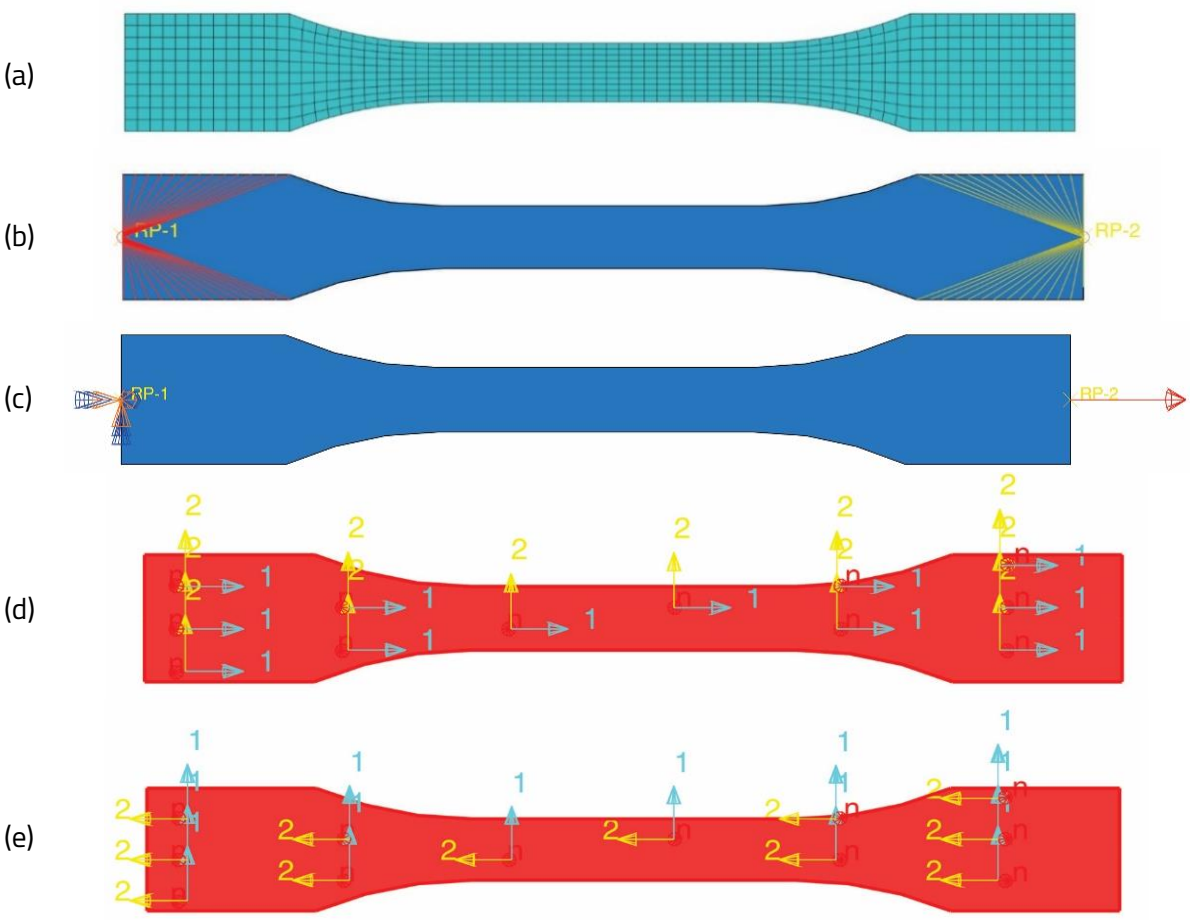

Figura 5.3. Numerical model for simulation of the tensile test: (a) finite element model, (b) coupling constraint, (c) defining of load and boundary condition, (d) material axis 1 is parallel to the specimen length, and (e) material axis 2 is parallel to the specimen length. [31].

The finite element model of the tensile specimen is shown in figure 5.9(a). Two coupling constraints controlled by two reference points were defined to simulate the fixing of the tensile specimen in the clamping jaws of the tensile machine and for applying of the tensile force to the other end of the bone shape specimen (fig. 5.9 b). All layers made of carbon-aramid/ epoxy composite material have

the same thickness of 0.325 mm considering that the average thickness of the composite is equal to 2.6 mm. The orientation angle of the reinforcement carbon-aramid woven fabric was considered the same in all layers.

5.3.2. Simulation of the bending test of the specimen made of laminated composite material reinforced with carbon-aramaid hybrid fabric

In figure 5.11 the numerical model used to simulate the stress and strain distributions in the bending test by using the three point method is presented.
simulate the stress and strains distributions in bending test by using the three point's method. The finite element model contains 320 shell elements of type S4R and it is shown in figure 5.11(a). The concentrated force is applied to the reference point located at midpoint of the flexural specimen (figure 5.11.b). The laminated composite material assigned to the flexural specimen, was defined the same like for simulation of the tensile test.

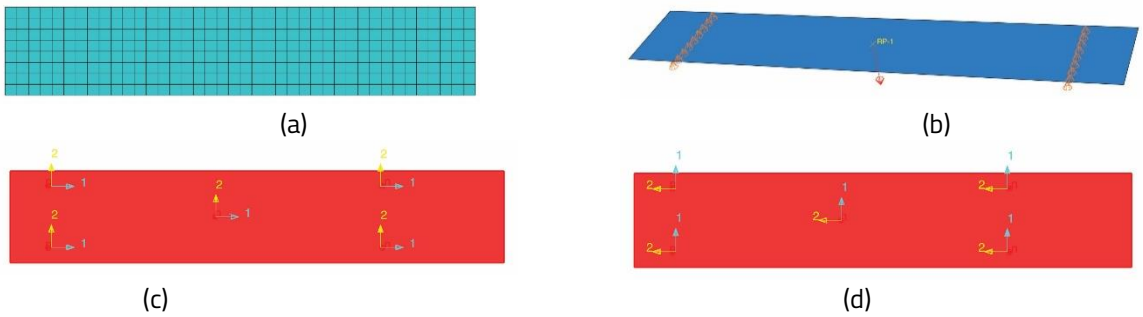

Figure 5.4. Numerical model for simulation of the bending test: (a) finite element model, (b) load and boundary conditions, (c) material axis 1 is parallel to the specimen length, and (d) material axis 2 is parallel to the specimen length. [31].

5.4. Experimental results

5.4.1. Elastic and tensile mechanical properties of carbon-aramid hybrid fabric reinforced composite material

Table 5.1 summarizes the tensile test results recorded by the test machine.

Table 5.1. Tensile properties for carbon-aramid composite material [31].

Specimen direction	Specimen code*	Dimensions of cross-section		Young's modulus	Maximum force	Tensile strength	Maximum strain ε_{max} at F_{max}	Poisson's ratio
		b (mm)	h (mm)	E (MPa)	F_{max} (N)	σ_{max} (MPa)		ν
Warp (R)	CK801R	10.20	2.60	35882	10775	406	0.0136	0.155
	CK802R	10.34	2.57	36108	11722	441	0.0117	0.119
	CK803R	10.33	2.66	36574	10434	380	0.0097	0.151
	CK804R	10.48	2.68	35458	11093	395	0.0108	0.122
	CK805R	10.46	2.78	32205	12013	413	0.0163	0.158
Average (stdev)				35245 (1747)	11207 (654)	407 (23)	0.0124 (0.0026)	0.141 (0.019)
Weft (F)	CK801F	10.60	2.74	33721	11127	383	0.0113	0.099
	CK802F	10.5	2.65	33627	10379	373	0.0107	0.0106
	CK803F	10.61	2.82	35107	11760	393	0.0101	0.118
	CK804F	10.52	2.74	33928	9741	338	0.0102	0.106
	CK805F	10.6	2.78	31747	11016	374	0.0111	0.102
Average (stdev)				33626 (1207)	10805 (770)	372 (21)	0.0107 (0.0005)	0.106 (0.007)

* The last letter specimen code indicates the direction of the tensile specimen: R – warp direction; F – weft direction.

In order to compute the Poisson ratio ν_{12} in the reinforcement plane with carbon-aramid woven fabric, the curve of the transverse strain ε_t related to the longitudinal strain ε_l was plotted for each specimen like is shown in figure 5.14.

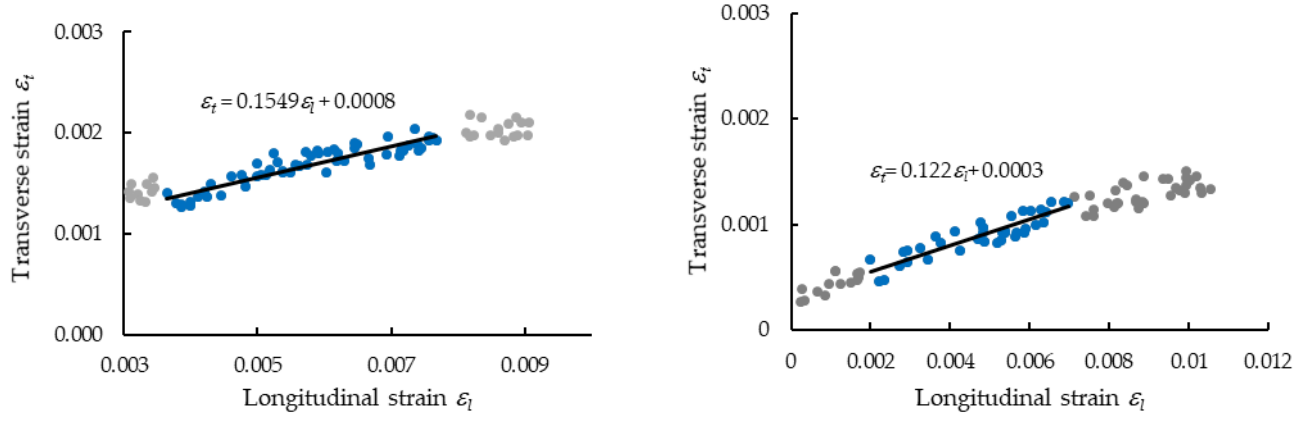

(**a**) (**b**)

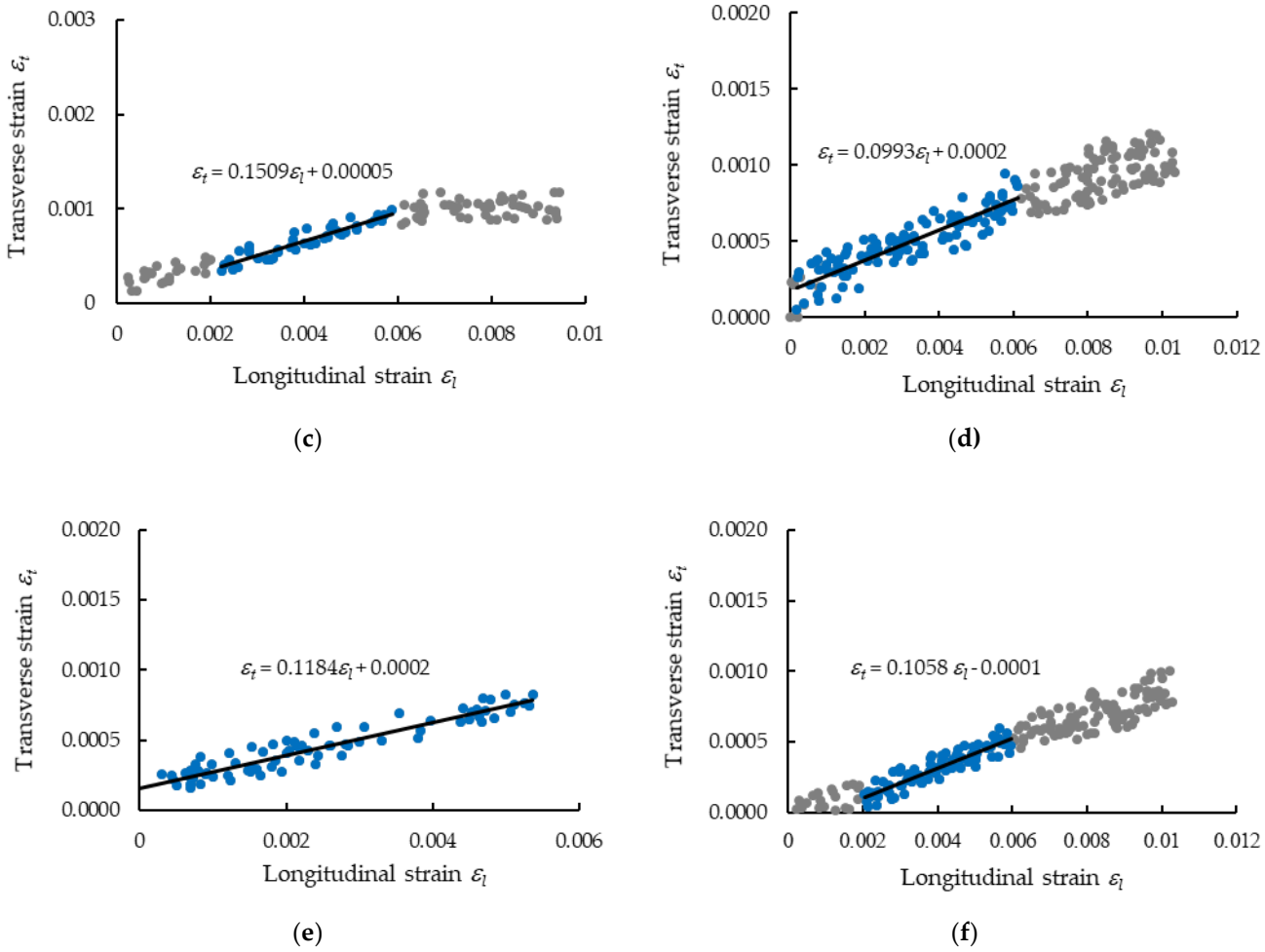

Figure 5.14. Curves of transverse strain ε_t related to longitudinal strain ε_l for determining Poisson' ratio ν12 by means of DIC method with respect to the both directions of carbon - aramid reinforcement fabric: (a) - (c) warp direction, and (d) - (f) weft direction [31].

5.4.2. Elastic and mechanical bending characteristics of carbon-aramid hybrid fabric reinforced composite material

After processing of the experimental data according to the European standard EN-ISO 14125 [41], the flexural properties (flexural modulus of elasticity, flexural strength) are determined and the results are synthesized in table 5.2.

Table 5.2. Flexural properties for carbon-aramid composite material [31].

Specimen direction	Specimen code*	Dimensions of cross-section		Flexural modulus of elasticity	Maximum force	Maximum stress	Maximum displacement
		b (mm)	h (mm)	E (MPa)	F_{max} (N)	σ_{max} (MPa)	v_{max} at F_{max} (mm)
Warp (R)	CK801R	14.99	2.55	29331	435	429	5.376
	CK802R	14.92	2.58	28846	396	382	4.686
	CK803R	14.96	2.52	29088	439	443	4.916
	CK804R	14.96	2.52	29409	418	422	5.016
	CK805R	14.98	2.58	30042	430	414	4.701
	Average (stdev)			29343 (449)	424 (17)	418 (23)	4.939 (0.282)
Weft (F)	CK801F	15.06	2.72	24899	377	325	5.400
	CK802F	14.88	2.56	29557	357	351	5.106
	CK803F	14.98	2.7	24767	412	362	4.435
	CK804F	14.93	2.61	27456	356	336	5.354
	CK805F	14.85	2.61	27741	413	392	5.222
	Average (stdev)			26884 (2039)	396 (28)	363 (26)	5.106 (0.391)

*The last letter specimen code indicates the direction of the tensile specimen: R – warp direction; F – weft direction.

5.4.3. Impact properties of carbon-aramid hybrid fabric reinforced composite material

The average values of the impact properties and their corresponding stdev values are shown in table 5.3 for each set of impact specimens: one set of specimens whose length is parallel to the warp direction of the reinforcement carbon-aramid woven fabric; another set of specimens whose length is parallel to the weft.

Table 5.3. Results obtained by Charpy impact testing [31].

Direction of the specimen	Impact failure energy W (J)	Impact strength (kJ/ m2)
Warp direction (R)	2.79 (0.23)	90.49 (5.88)
Weft direction (F)	2.43 (0.12)	80.36 (3.19)

*The values shown in the brackets represent stdev values.

5.5. Theoretical results

5.5.1. Results obtained by analytical method

Using the calculation formulas presented in chapter 4, the values presented in table 5.4 are obtained for the mechanical and elastic characteristics of the composite material reinforced with carbon-aramid hybrid fabric.

Table 5.4. Characteristics of the carbon-aramid layer computed by using the analytical method and considering the results obtained in tensile tests [31].

Direction	Thickness t_k of the layer (mm)	Elastic characteristics of the layer			Terms of the stiffness matrix $[Q]_k$ of the composite layer		
		E_1 (MPa)	E_2 (MPa)	ν_{12}	Q_{11} (MPa)	Q_{12} (MPa)	Q_{22} (MPa)
Warp (R)	0.325	35245	33626	0.141	35927.625	4833.095	34277.268
Weft (F)		33626	35245	0.106	34027.525	3780.581	35665.857

Table 5.5 shows the results obtained using the analytical method considering the experimental results during the bending test using the three-point method.

Table 5.5. Characteristics of the carbon-aramid layer computed by using the analytical method and considering the results obtained in bending tests [31].

Direction	Thickness t_k of the layer (mm)	Elastic characteristics of the layer			Terms of the stiffness matrix $[Q]_k$ of the composite layer		
		E_1 (MPa)	E_2 (MPa)	ν_{12}	Q'_{11} (MPa)	Q'_{12} (MPa)	Q'_{22} (MPa)
Warp (R)	0.325	29343	26884	0.141	29886.942	3860.913	27382.359
Weft (F)		26884	29343	0.106	27218.791	3149.092	29708.413

Using relations (4.27), the components of the two stiffness matrices [A] and [D] are calculated, and the results are presented in table 5.6.

Table 5.6. Stiffness matrix components and equivalent modulii of elasticity of the carbon-aramid laminated composite material, computed by using the analytical method [31].

Direction	Stiffness matrix components						Equivalent tensile modulus of elasticity E (MPa)	Equivalent flexural modulus of elasticity E′ (MPa)
	A_{11} (N/mm)	A_{12} (N/mm)	A_{22} (N/mm)	D_{11} (N · mm)	D_{12} (N · mm)	D_{22} (N · mm)		
Warp (R)	93411,83	12566,05	89120,90	43774,41	5654,95	40106,03	33626,78	29342,55
Weft (F)	88471,57	9829,51	92731,23	39866,46	4612,37	43512,92	35246,16	26884,99

5.5.2. Results obtained by FEA

In figure 5.17, it is plotted the results obtained by using the numerical model of the tensile specimen loaded on warp direction of the reinforcement carbon-aramid fabric. Figure 5.18 shows the results obtained by FEA for the tensile specimen loaded on weft direction of the reinforcement carbon-aramid fabric.

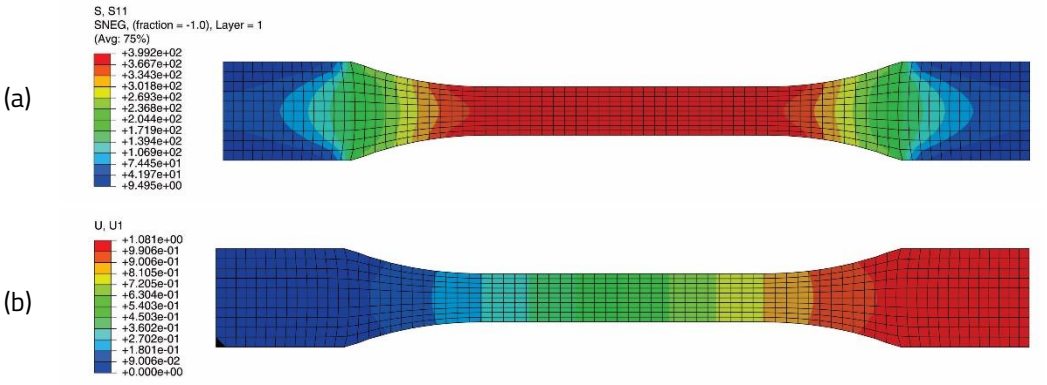

Figure 5.17. Results obtained by simulation of the tensile test of the specimen whose length is parallel to the warp direction of the reinforcement carbon-aramid fabric: (a) normal stress, and (b) displacement on specimen direction.

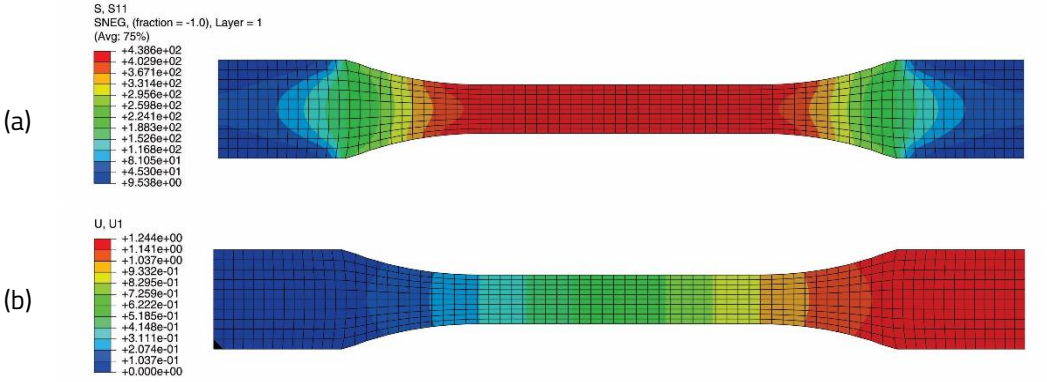

Figure 5.18. Results obtained by simulation of the tensile test of the specimen whose length is parallel to the weft direction of the carbon-aramid fabric: (a) normal stress, and (b) displacement on specimen direction.

In figure 5.20 and figure 5.21, it is presented the results obtained by simulation of the bending test for the specimen whose length is parallel to the warp direction and respectively, for the specimen whose length is parallel to the weft direction of the carbon-aramid woven fabric

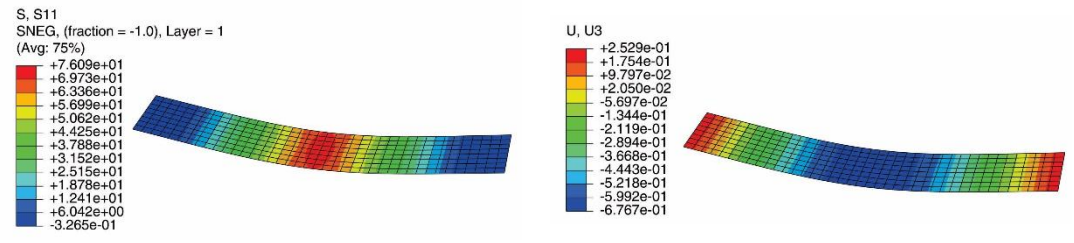

(a) (b)

Figure 5.20. Results obtained by simulation of the bending test of the specimen whose length is parallel to the warp direction of the carbon-aramid fabric: (a) normal stress on specimen direction, and (b) vertical displacement.

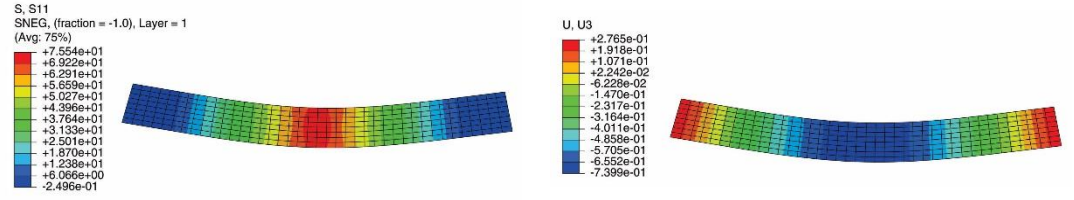

(a) (b)

Figure 5.21. Results obtained by simulation of the bending test of the specimen whose length is parallel to the weft direction of the carbon-aramid fabric: (a) normal stress on specimen direction, and (b) vertical displacement.

5.6. Comparison of the results

Table 5.7 summarizes the values of the equivalent tensile modulus of elasticity, corresponding to the warp and weft directions of the carbon-aramid hybrid reinforcing fabric.

Table 5.7. Comparison of the results obtained for the tensile moduli of elasicity in case of tensile loading [31].

Direction	Equivalent tensile modulus of elasticity E_t (MPa)			Error (%)		
	AnM*	FEA	Exp*	FEA vs AnM	Exp vs AnM	Exp vs FEA
Warp (R)	35246,16	35311	35245	0,18	0,003	0,19
Weft (F)	33626,78	33684	33626	0,17	0,002	0,17

*AnM – analytical method; Exp – experimental results.

The values of the equivalent flexural moduli of elasticity corresponding to the warp and weft directions of the reinforcement carbon-aramid fabric, are synthesized in table 5.8.

Table 5.8. Comparison of the results obtained for the flexural moduli of elasticity in case of bending loading [31].

Direcția țesăturii	Equivalent flexural modulus of elasticity E' (MPa)			Error (%)		
	AnM*	FEA	Exp*	FEA vs AnM	Exp vs AnM	Exp vs FEA
Warp (R)	29342,55	29387,40	29343,00	0,15	0,002	0,15
Weft (F)	26884,99	26877,70	26884,00	0,03	0,004	0,02

*AnM – analytical method; Exp – experimental results.

5.7. Conclusion

From the tensile tests it can be concluded that the composite material reinforced with carbon-aramid hybrid fabric has the longitudinal modulus of elasticity E in the warp direction about 4% higher than in the weft direction corresponding to the reinforcement fabric. In the warp direction of the carbon-aramid hybrid fabric, the maximum normal tensile stress for the five tensile tested specimens is 407 MPa, which is about 9.4% higher than the maximum normal stress recorded in the case of tensile stress in the weft direction of the hybrid fabric.

For the bending test by the three-point method, it can be concluded that for the samples run parallel to the warp direction of the reinforcing fabric, better properties were obtained than for those run parallel to the weft direction, namely, approximately 15% higher in with respect to the maximum normal stress and approximately 9% higher with respect to the longitudinal modulus of elasticity. For the specimens whose length is parallel to the warp direction of the carbon-aramid fabric, the average value of the maximum deflection for the five tested specimens is 4.939 mm for the average force value of 424 N. For the specimens whose length is parallel to the weft direction , the mean values for maximum deflection and maximum force were 5.106 mm and 396 N, respectively.

After the impact test by Charpy test, it is found that no specimen completely ruptured, but approximately 12% higher impact resistance (toughness) can be observed for the specimens flowed parallel to the warp direction of the carbon-aramid hybrid fabric than for those debited parallel to the weft direction. In terms of failure modes, delaminations between layers, fiber breaks in some layers, debonding at the fiber-resin interface, as well as cracks in the matrix were found.

In this section, only a summary of the conclusions of the doctoral thesis is presented.

6. Mechanical Behaviour of the Carbon-Aramid Composite Materials Subjected Low-Velocity Impact Loading

6.1. Materials tested

Two sets of specimens were manufactured for the low-velocity impact testing. All specimens are square panels having the dimensions 70 mm x 70 mm. The first set of samples was cut from a composite panel reinforced just with carbon-aramid hybrid fabric, which having eight layers, was manufactured by hand-layup technology, resulting in an average thickness of approximately 2.6 mm. The second set of specimens was cut from a sandwich composite panel, having both upper and bottom faces made of three layers of composite material reinforced with carbon-aramid hybrid fabric and a rubber core whose thickness is 2 mm [66]. The same technology described above was used resulting in an average sample thickness of approximately 3.75 mm.
From the same batch of specimens fabricated for the low-velocity impact test, ten specimens of each set were fully immersed in water and held to saturation. To control the energy level during the tests, impact tests were performed for the following configurations: (i) for the impact energy level of 50 J, the mass of the impact hammer was 10.728 kg and the velocity at impact with the plate was 3.05 m/s; (ii) for the impact energy of 25 J, the mass of the impact hammer was 10.728 kg and the velocity at impact with the plate was 2.16 m/s.

Table 6.1. Material structure and number of specimens for the low-velocity impact testing [60].

Composite material	Specimen codes *	Material structure of the specimen	Type of specimens	Number of specimens tested	
				Impact energy 25 J	Impact energy 50 J
Carbon-aramid / epoxy Epolam 2031	CK801...CK810	Panel having eight layers reinforced with carbon-aramid hybrid fabric	Dried specimens	5	5
	CK811...CK815, CK818...CK822		Wet specimens	5	5
Carbon-aramid with rubber core / epoxy Epolam 2031	CK2R17...CK2R26	Sandwich panel with both faces made of composite material containing three layers reinforced with carbon-aramid hybrid fabric and a rubber core	Dried specimens	5	5
	CK2R01...CK2R10		Wet specimens	5	5

*CK8XX: CK8 – eight layers of aramid-carbon hybrid fabric, xx – specimen number; CK2RXX: CK – composite material reinforced with aramid-carbon fabric, 2R – rubber core having thickness of 2 mm, XX – specimen number.

6.2. Experimental work method

6.2.1. Low-velocity drop impact test

The low-velocity drop impact tests were carried out by Instron CEAST 9340 impact machine (Norwood, MA, USA) shown in figure 6.3, at the room temperature (20 °C ± 2 °C). The testing system consists of an impact hammer equipped with a force cell (maximum 22 kN), clamping fixtures and data acquisition system (fig. 6.3.). The main technical characteristics of Instron CEAST 9340 machine are: maximum impact energy of 405 J; maximum impact velocity of 4.65 m/s; mass of the drop weight system is in the range 2÷70 kg; drop weight is in the range 0.03÷1.10 m.

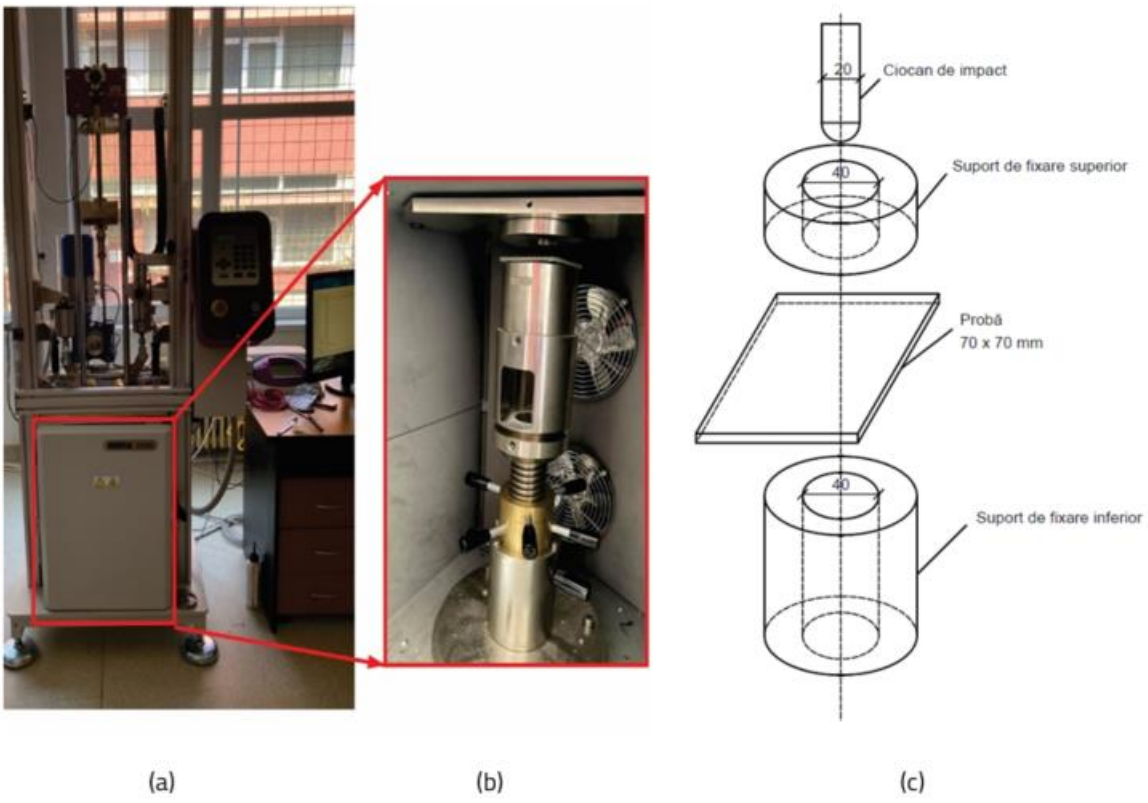

Figure 6.3. Low-velocity impact test setup: (a) photo of Instron CEAST 9340 drop weight impact machine; (b) photo of the fixture devices of the specimen during the impact test; (c) scheme with dimensions for the impact specimen and for the devices of the impact machine [60].

6.2.2. Determination of moisture absorption in carbon-aramid hybrid fabric reinforced composite materials

As shown in figure 6.4, the samples were completely covered by water, being placed in a vessel filled with water and placed on an aluminium support, which allows directly contact with water for all surfaces of each specimen, so that these specimens were not in contact with the walls or with the bottom of the vessel. To maintain the immersion conditions, the water was refreshed weekly.

To maintain immersion conditions, the water was refreshed at weekly intervals. For each set of specimens, the water immersion time was until saturation, that is, until the mass of water absorbed inside the composite material stabilized. During the immersion period, the samples were weighed periodically, using the same analytical balance, and the mass of the wet samples was recorded, and the data was recorded until the mass of the samples stabilized.

(a) (b)

Figure 6.4. Impact specimens immersed in water: (a) top view; (b) lateral view [60].

6.3. Results and discussion on the low velocity impact behavior of the tested composites

6.3.1. Experimental results obtained in low velocity impact tests for dry samples

Figure 6.7 presents comparative results between 25 J impact level and 50 J impact level obtained in low-velocity impact tests, regarding the following variation curves: impact force related to time $(F-\mathrm{t})$, velocity-time $(v-\mathrm{t})$, displacement-time $(\delta_{max}-\mathrm{t})$ and impact force-displacement $(F-\delta_{max})$.

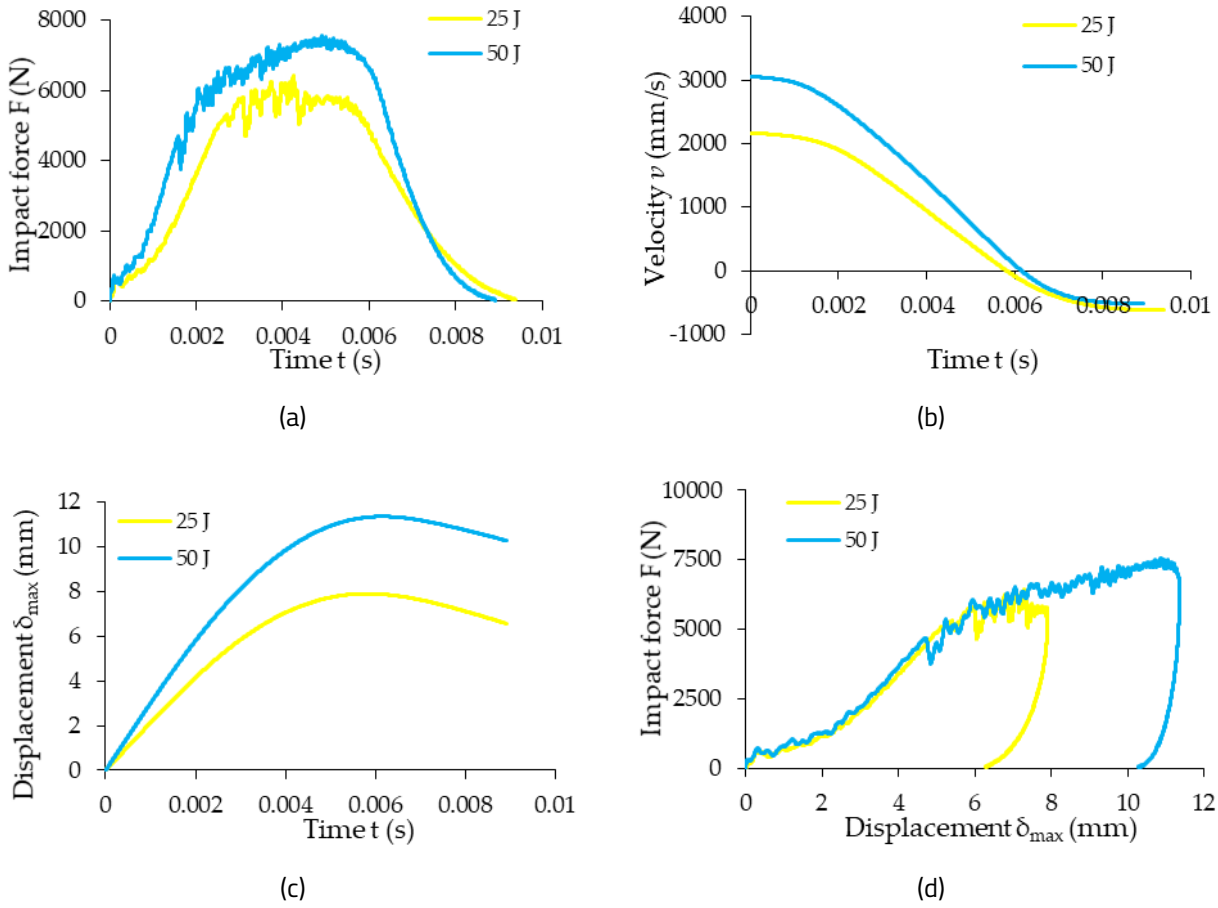

Figure 6.7. The comparative results obtained in the low-velocity impact test: (a) the impact force-time $(F-\mathrm{t})$; (b) velocity - time $(v-\mathrm{t})$; (c) maximum displacement - time $(\delta_{max}-\mathrm{t})$; (d) impact force - maximum displacement $(F-\delta_{max})$ [60].

It can be noted that the maximum force recorded is up to 32.7 % higher in case of 50 J impact energy comparing to the one recoded for the 25 J impact energy and also, the maximum displacement recorded for the 50 J impact energy is up to 45 % higher than the one recorded for the 25 J impact energy.

Figure 6.10 presents comparatively the results obtained for 25 J and 50 J impact energy levels, obtained when the low-velocity impact tests were carried-out on the sandwich hybrid composite specimens with rubber core, regarding the following variation curves: impact force-time $(F-t)$, velocity-time $(v-t)$, displacement-time $(\delta_{max}-t)$ and impact force-displacement $(F-\delta_{max})$.

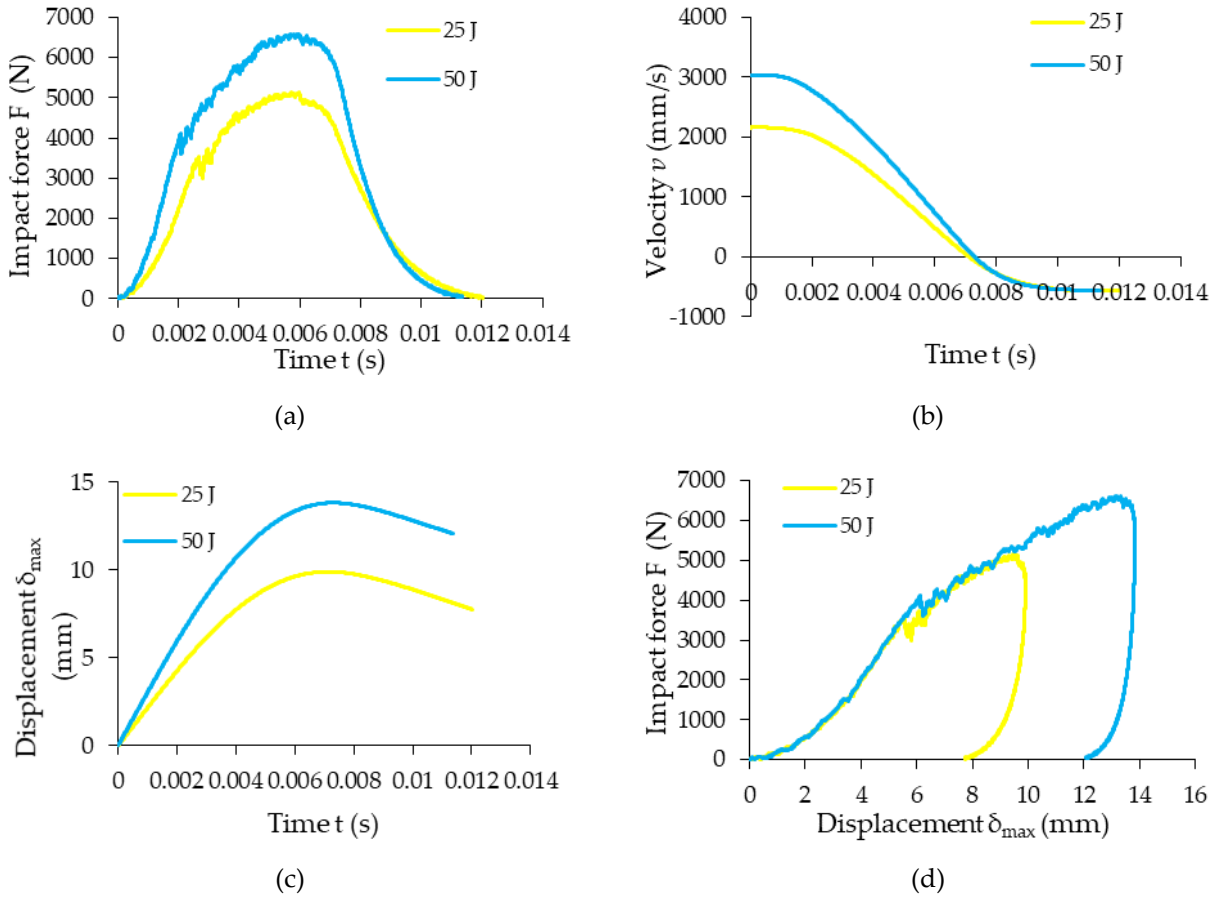

Figure 6.10. Comparative results obtained for sandwich hybrid composite specimens with a rubber core in low-velocity impact tests regarding: (a) impact force-time $(F-\mathrm{t})$; (b) velocity-time $(v-\mathrm{t})$; (c) displacement-time $(\delta_{max}-\mathrm{t})$; (d) impact force-displacement $(F-\delta_{max})$ [60].

It can be noted that the maximum force recorded is up to 27.7 % higher in case of 50 J impact energy comparing to the one recoded for the 25 J impact energy and also, the maximum displacement recorded for the 50 J impact energy is up to 39 % higher than the one recorded for the 25 J impact energy.

Also, a very important measured parameter during the low-velocity impact tests is the energy absorbed by the composite materials tested during impact tests. The values of the energy absorbed is an important factor in the design of structures manufactured from different composite materials. Therefore, figure 6.12 presents comparatively the variation of the energy absorbed related to time for both impact energy levels of 25 J and 50 J.

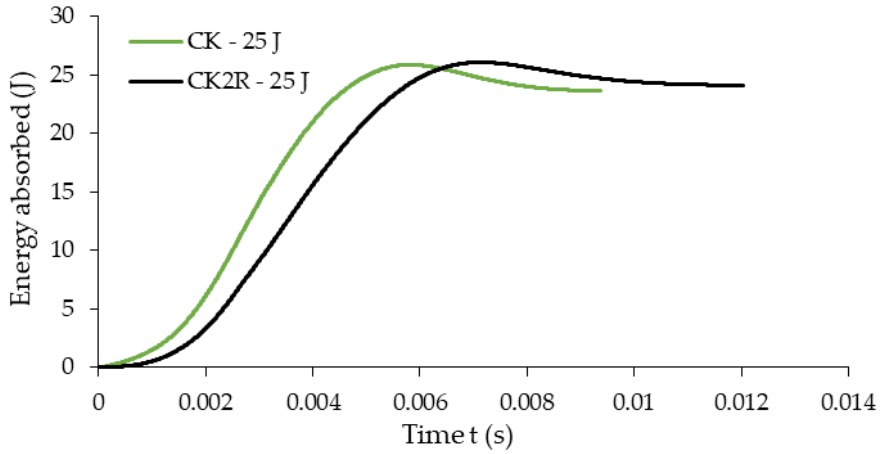

(a)

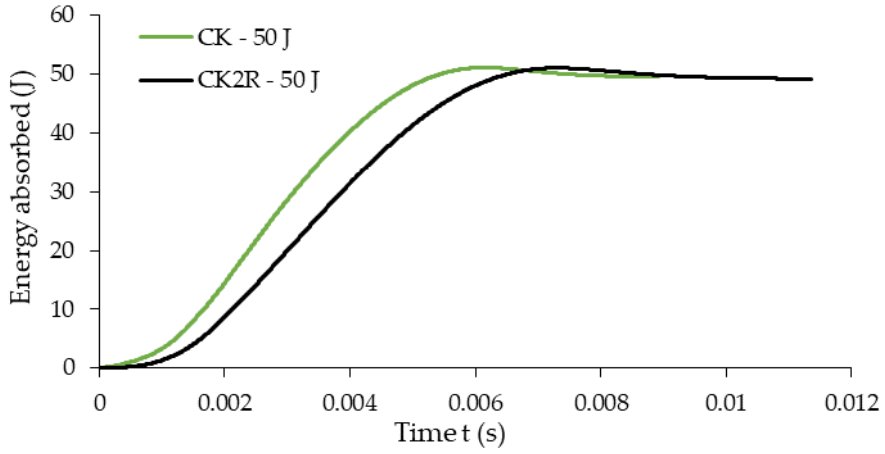

(b)

Figure 6.12. Comparative analysis of the variation of the energy absorbed by the material related to the time during the impact, for the both type of specimens tested at two different impact energy levels: (a) 25 J; (b) 50 J [60].

In conclusion, the replacement of two central layers of the layered composite material, reinforced with carbon-aramid fabric, by the rubber core leads to a delay in the absorption of strain energy during impact, while the energy absorbed is the same as that absorbed by the materials composites without a rubber core (fig. 6.12).

6.3.2. Absorption data

It may be noted that after approximately 8440 hours of immersion in water, the absorption curve tends asymptotically to the equilibrium value of the absorbed water content of $M_m = 2.42\ \%$ for the composite specimens without rubber core, The equilibrium value of the absorbed water content is $M_m = 4.97\ \%$ after approximately 10513 hours of immersion in water for the specimens with rubber core. The initial portion of the absorption curve was approximated with a linear function graphically plotted as a line. In conclusion the moisture content M_m at saturation of the CK composite materials

involved in this study is approximately 48.70 % lower than the corresponding value M_m at saturation recorded in the case of the CK2R composite materials.

6.3.3. Experimental results obtained in low-velocity impact tests after immersion in water of composite materials reinforced with carbon-aramid hybrid fabric

After immersion in water until saturation is reached (when the absorbed moisture content tends to a constant value), the samples were subjected to the low-velocity impact test under the same test conditions as those presented in sub-chapter 6.3.1. In figure 6.18 presents comparatively the results obtained for 25 J and 50 J impact energies, in the low-velocity impact tests, for CK composite specimens reinforced with eight layers of carbon-aramid hybrid fabric, regarding the following curves: impact force-time $(F-t)$, velocity-time $(v-t)$, displacement-time $(\delta_{max}-t)$ and impact force-displacement $(F-\delta_{max})$. For the graphic representation shown in figure 6.18, it was chosen for the impact energy of 25 J to represent the curves obtained for sample CK814, respectively the curves obtained for sample CK820 for the impact energy of 50 J, considering them as the average curves.
It can be seen that the maximum force recorded for the wet CK samples is up to 14% higher for the impact energy of 50 J than the value obtained for the wet CK samples tested at an impact energy of 25 J. Also from figure 6.18 (b) it can be seen that recoil occurs only for wet CK samples subjected to an impact energy of 25 J.

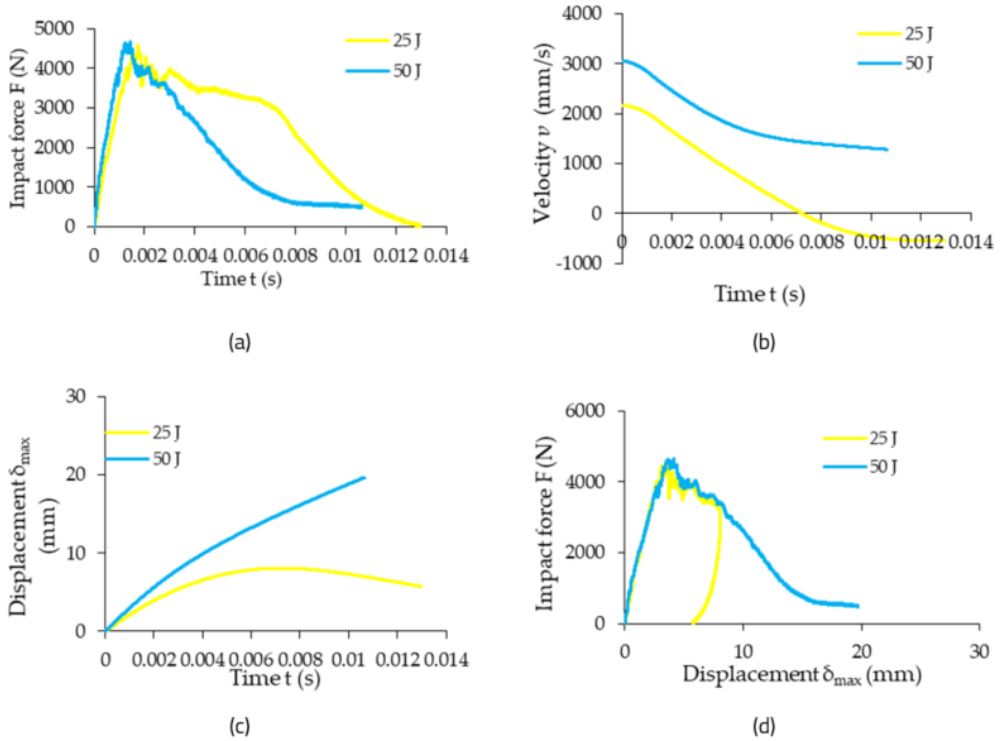

Figure 6.18. Comparative results obtained for CK composite specimens reinforced with eight layers of carbon-aramid hybrid fabric, after 8440 hours of immersion in water, for low-velocity impact tests at 25 J and 50 J impact energies: (a) impact force-time $(F-t)$; (b) velocity-time $(v-t)$; (c) displacement-time $(\delta_{max}-t)$; (d) impact force-displacement $(F-\delta_{max})$.

In figure 6.20 presents the comparative results obtained for 25 J and 50 J impact energies in the low-velocity impact tests for CK2R composite specimens having rubber core, regarding the following variation curves: impact force-time $(F-t)$, velocity-time $(v-t)$, displacement-time $(\delta_{max}-t)$ and impact force-displacement $(F-\delta_{max})$. For the graphs plotted in Figure 21, it was chosen the curves obtained for CK2R10 and CK2R4 impact specimens were selected for the impact energies of 25 J and 50 J respectively, while the curves for sample considering them as average curves.

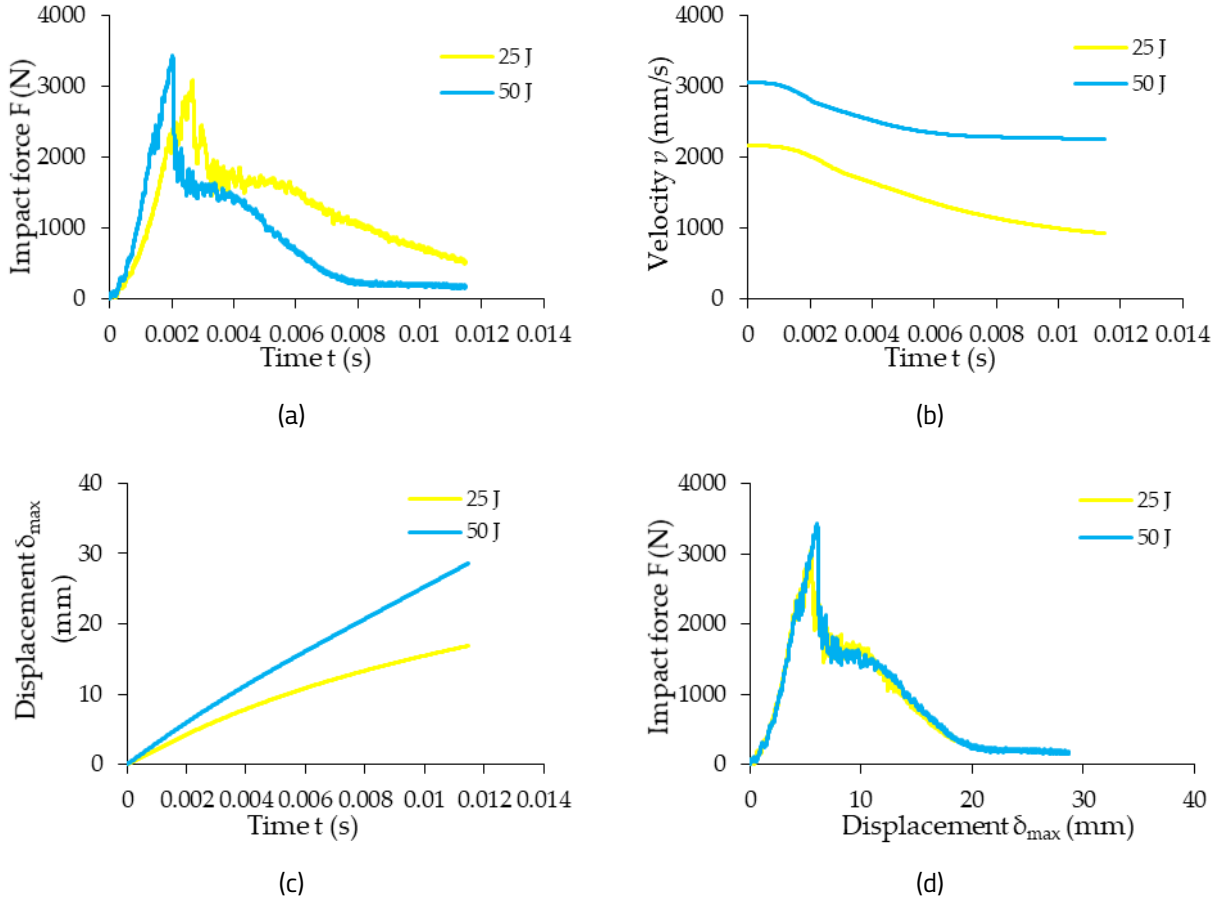

Figure 6.20. Comparative results obtained CK2R sandwich composite specimens with a rubber core after 10513 hours of immersion in water, in low-velocity impact tests for impact energies of 25 J and 50 J: (a) impact force-time $(F-t)$; (b) velocity-time $(v-t)$; (c) displacement-time $(\delta_{max}-t)$; (d) impact force-displacement $(F-\delta_{max})$.

From the analysis of the graphs in figure 6.20(a), it can be seen that the maximum force recorded for the wet CK2R samples is up to 13% higher for the impact energy of 50 J, than the value obtained for the wet CK2R samples, tested at an energy of impact 25 J. Also, from figure 6.20 (b) it can be seen that the recoil did not occur for any of the impact energies.

For both 25 J and 50 J impact energy, all rubber-core hybrid composite material specimens immersed for 10513 hours in water were completely punctured.

6.3.3. Effects of water absorption on the impact behavior of composites reinforced with carbon-aramid hybrid fabric

Figure 6.22 presents comparatively the results obtained for dried and wet CK composite specimens in the low-velocity impact tests, regarding the following curves: impact force-time $(F-t)$, velocity-time $(v-t)$, displacement-time $(\delta_{max}-t)$, impact force-displacement $(F-\delta_{max})$.

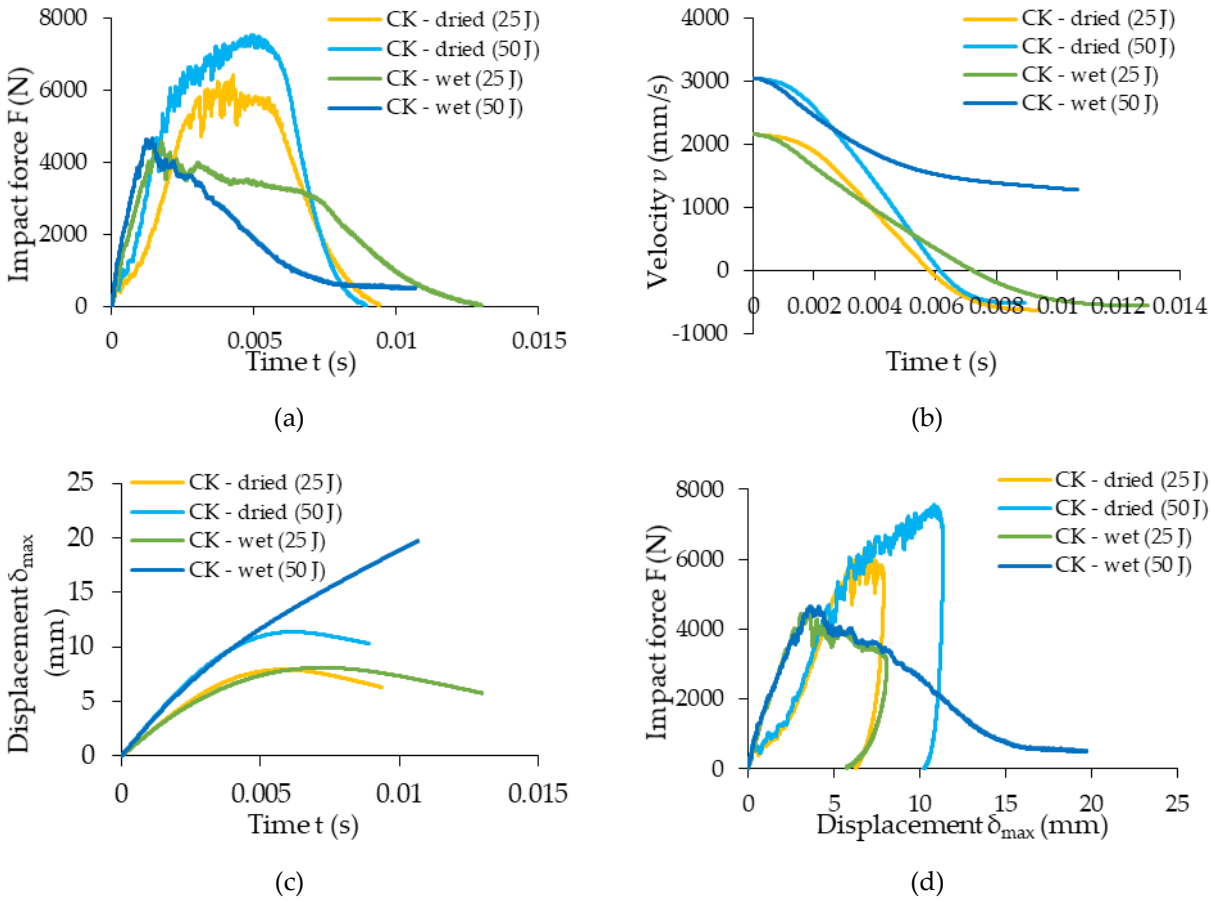

Figure 6.22. Comparative results obtained for wet and dried CK composite specimens for 25 J and 50 J impact energies: (a) impact force-time $(F-t)$; (b) velocity-time $(v-t)$; (c) displacement-time $(\delta_{max}-t)$; (d) impact force-displacement $(F-\delta_{max})$.

Analyzing the curves in figure 6.22(a), it can be seen that the maximum force recorded for the dry samples of type CK, for the impact energy of 50 J, is up to 67% higher than the wet CK samples, for the same impact energy and up to 39% higher for those tested at 25 J impact energy. The maximum displacement recorded for the dry CK samples for the 25 J impact energy is not significantly higher than the maximum displacement recorded for the wet CK samples, being about 0.02 mm higher. On the other hand, the maximum displacement recorded at 50 J impact energy for dry CK samples is 3.60 mm higher than the maximum displacement recorded for both dry CK and wet CK samples tested at impact energy of 25 J.

In figure 6.24 presents comparatively the results recorded for wet and dried CK2R composite specimens with rubber core, in the low-velocity impact tests, regarding the following variation curves: impact force-time $(F-t)$, velocity-time $(v-t)$, displacement-time $(\delta_{max}-t)$, impact force-displacement $(F-\delta_{max})$.

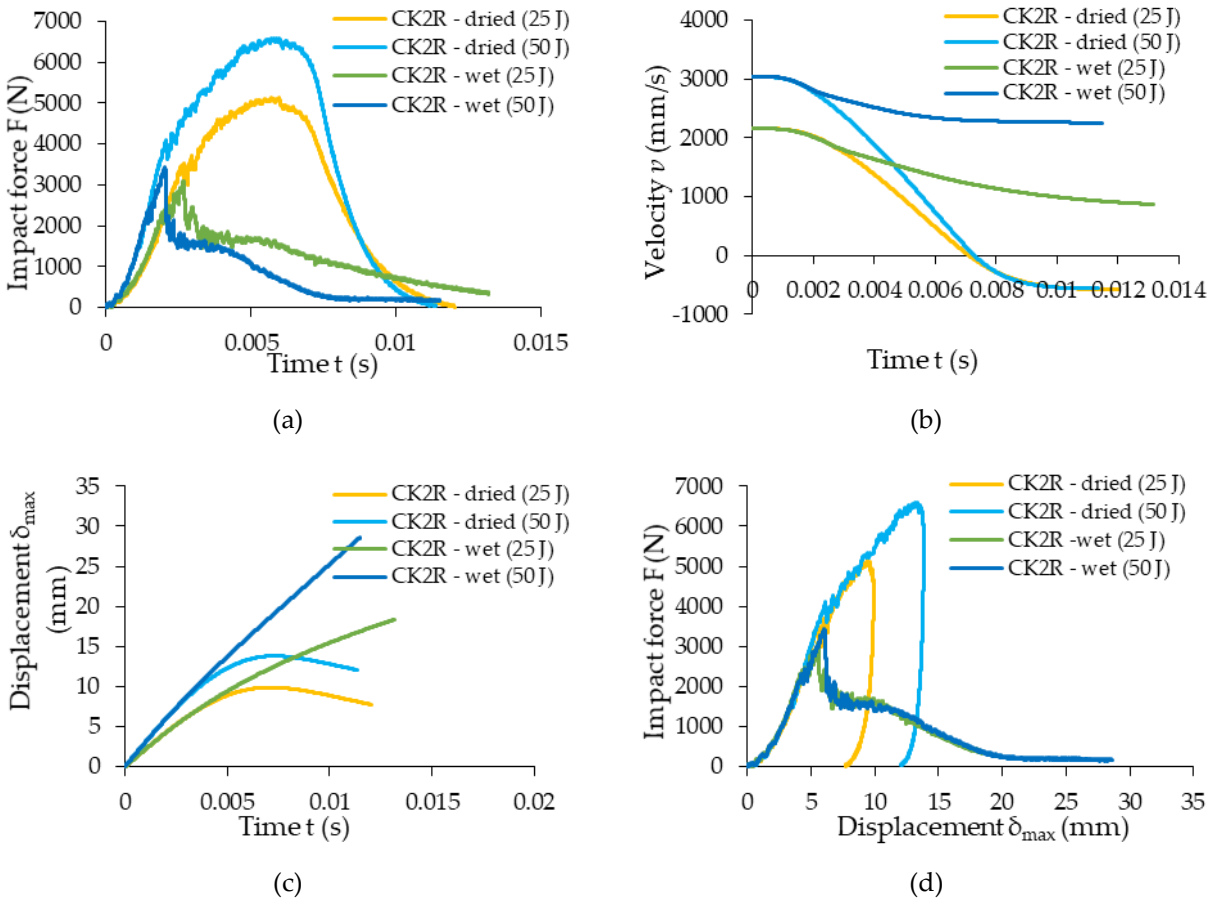

Figure 6.24. Comparative results between wet and dried CK2R composite specimens for 25 J impact level and 50 J impact level: (a) impact force-time $(F-t)$; (b) velocity-time $(v-t)$; (c) displacement-time $(\delta_{max}-t)$; (d) impact force-displacement $(F-\delta_{max})$.

6.3.4. Failure modes

None of the layers of the dry composites tested completely ruptured during the low-velocity impact test for any of the impact energies. As a result, the impactor did not completely penetrate any of the dry hybrid composite plates. In the case of wet specimens without a rubber core, the specimens are not completely punctured for the 25 J impact energy, while for the 50 J impact energy, the specimens are completely punctured. For the wet rubber core samples, for both energy levels, the impactor completely penetrated the hybrid composite plates.

6.4. Conclusion

- from the low-velocity drop impact tests, carried out on specimens of layered composite materials reinforced with carbon-aramid hybrid fabric, with and without a rubber core, tested before immersion in water, the following main conclusions can be noted:
  - the replacement of two core layers reinforced with carbon-aramid fabric with the rubber core is a reliable solution for the applications of these types of composite materials in dried environments because the degradation of the impact properties is much more pronounced for the composite material with rubber core, after water absorption (chapters 6.3.1, 6.3.3);
  - from the point of view of the absorbed energy, there is a rather small difference between the two sets of samples, namely, for the impact energy of 25 J, in the case of dry samples of type CK2R the average value of the absorbed energy is only 0, 17% lower than that corresponding to dry samples of type CK; for the impact energy of 50 J, dry samples of type CK2R absorbed approximately the same amount of energy as dry samples of type CK (see chapter 6.3.1);
  - the maximum displacement recorded for dry samples of CK2R composite material with rubber core was approximately 26% and 22% higher than the maximum displacement recorded for dry samples CK without rubber core, for impact energies of 25 J and, respectively, of 50 J (see chapter 6.3.1);
- from the analysis of the effects of water absorption on the low-velocity impact behavior of composite materials reinforced with carbon-aramid hybrid fabric, the following main conclusions are drawn:
  - for the CK composite material reinforced only with carbon-aramid hybrid fabric, both in the case of those tested at impact before immersion, and in the case of the samples tested after 8440 hours of immersion in water, subjected to an impact energy of 25 J, the amount of absorbed energy is approximately the same, the difference being only 0.93% compared to the value recorded for dry ones (see chapter 6.3.3 and 6.3.4);
  - for the impact energy of 50 J, a significant difference can be observed in terms of the energy absorbed by the CK composite material, as follows: 49.79 J for the dry samples and 41.84 J for the samples tested after 8440 hours of immersion in water, the decrease being 16% (see chapter 6.3.3 and 6.3.4);
  - for CK2R samples with a rubber core, both in the case of those tested at impact before immersion, and in the case of samples tested after 10513 hours of immersion in water, subjected to an impact energy of 25 J, the absorbed energy is approximately the same, the difference being only 1.82% compared to the value recorded for dry ones (see chapter 6.3.3 and 6.3.4);

- for the impact energy of 50 J, a significant difference can be observed in terms of the energy absorbed by the CK2R composite material with a rubber core, as follows: 49.77 J for the dry specimens and 26.74 J for the tested specimens, respectively after 10513 hours of immersion in water, the decrease being 53.26% (see chapter 6.3.3 and 6.3.4);

In this section, only a summary of the conclusions of the doctoral thesis is presented.

7. RESEARCH ON THE MODELING AND TESTING OF THIN-WALLED BEAMS MADE OF CARBON-ARAMIDEHYBRID FABRIC REINFORCED COMPOSITE MATERIAL

7.1. Experimental analysis of deformation states and displacements in the case of beams made of composite material reinforced with carbon-aramid hybrid fabric, subjected to bending

7.1.1. Beams tested

For the bending test by the three-point method, four thin-walled beams, made of composite material reinforced with carbon-aramid hybrid fabric. The beam, having a rectangular section, with thin walls (in English, of the "box" type), was obtained by gluing two profiles with a U section, made of composite material based on Epolam 2031 epoxy resin, reinforced with carbon hybrid fabric -aramid [59]. For the manufacture of the two profiles with the U-shaped section, which make up the composite beam, two metal molds were used (fig. 7.1), over which the eight layers of carbon-aramid hybrid fabric, impregnated with Epolam 2031 type epoxy resin. The resin was pre-mixed with the Epolam 2031 hardener, the volume ratio of the mixture being equal to 100:33, according to the technical sheet of the epoxy resin [61].

Figure 7.1. U-type profile made of hybrid composite material obtained by manual layering technology ("lay-up" technology).

7.1.2. Three-point bending test combined with the digital image correlation method

For the three-point bending test, the testing machine produced by Walter&Bai (Switzerland) was used, the maximum force of which is 100 kN for the vertical force actuator. Figure 7.2 shows the static loading scheme of the hybrid composite beam and the cross-section sketch of the composite beams.

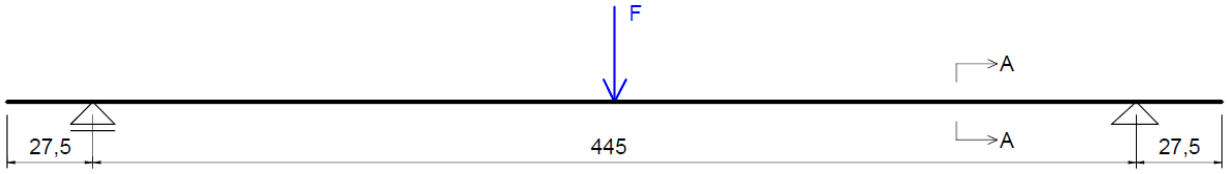

(a)

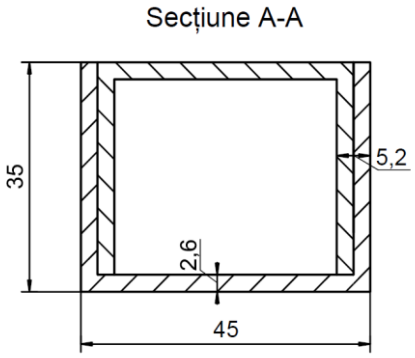

(b)

Figure 7.2. Three-point bending test setup: (a) static loading scheme; (b) cross-section of the composite beam (dimensions are in mm.).

For the accuracy of the results of the bending test by the three-point method, the testing machine produced by Walter&Bai and the 3D optical deformation analysis system for materials and components, by the DIC (digital image correlation) method, were simultaneously used to accurately determine the displacements of certain points, as well as the deformation field for the surface of the samples.

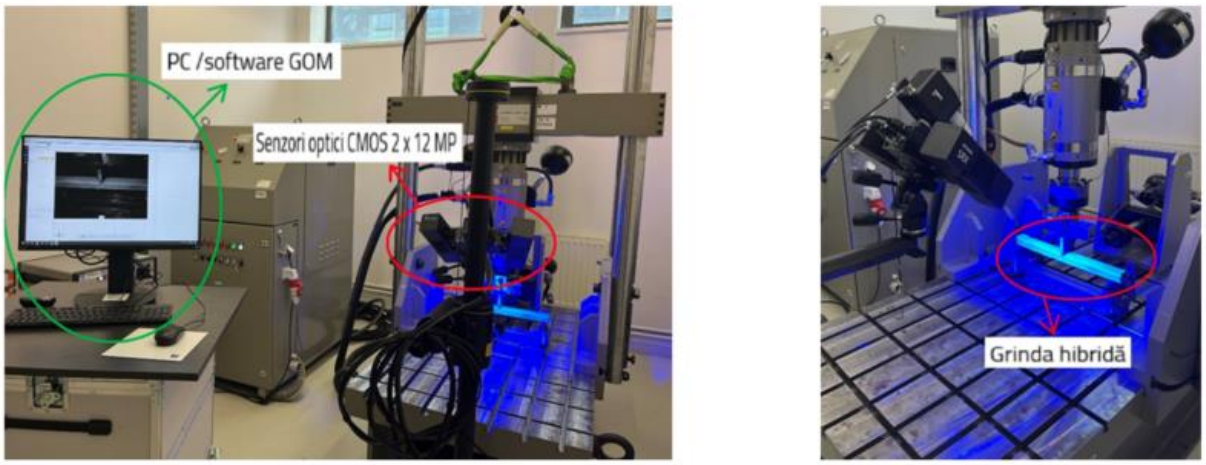

Figure 7.3. Bending test setup by the three-point method combined with the DIC method.

7.1.2. Flexural test results for thin-walled beams made of carbon-aramid hybrid fabric reinforced composite material

After processing the experimental data recorded by the test machine, the force variation curve was drawn as a function of the vertical displacement (arrow) at the middle of the beam (for all four tested beams (fig. 7.4). The vertical displacement recorded represents the displacement of the loading roller.

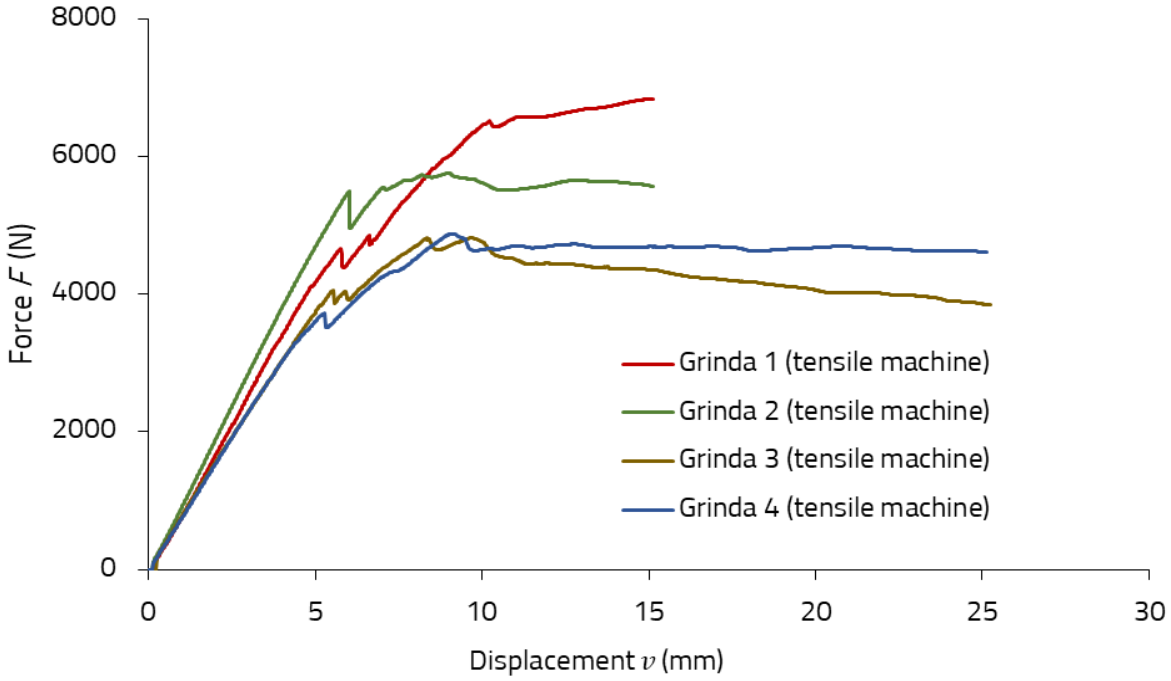

Figure 7.4. Force curve – vertical displacement at mid-beam ($F - v$) for tensile machine.

The experimental results obtained by the DIC method are calculated for an area of interest defined on the beam, and the results are displayed for certain points, which are chosen from this area of interest, namely points located as close as possible to the middle of the beam (fig. 7.5). Figure 7.5 shows the images taken during the bending test, for one of the tested beams (beam 2), in which the results regarding the evolution of vertical displacements in the points of interest, obtained with the digital image correlation method, up to a value of arrows about 1 mm.

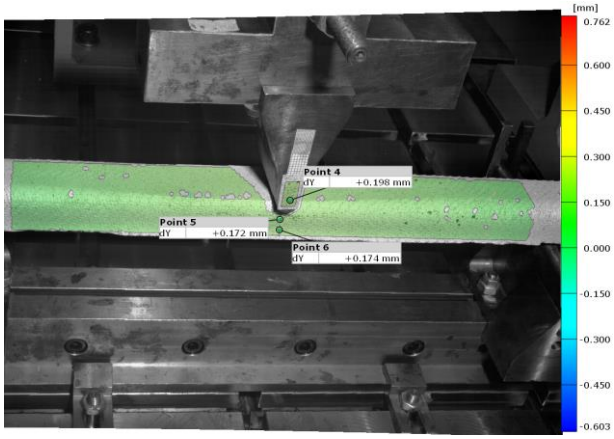

(a) Displacement v = 0,172 mm for F = 160,78 N

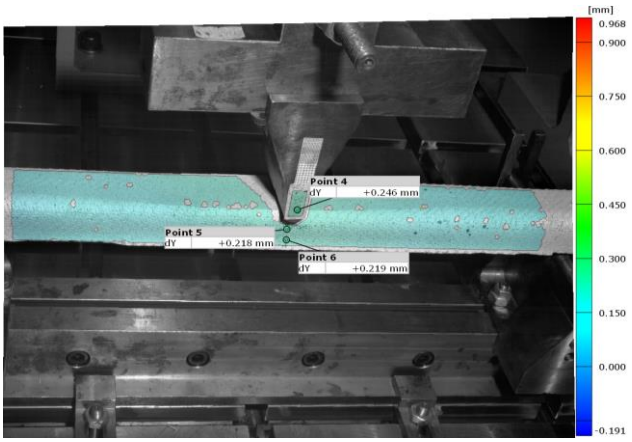

(b) Displacement v = 0,218 mm for F = 203,21 N

(c) Displacement $v = 0{,}265$ mm for $F = 246{,}17$ N

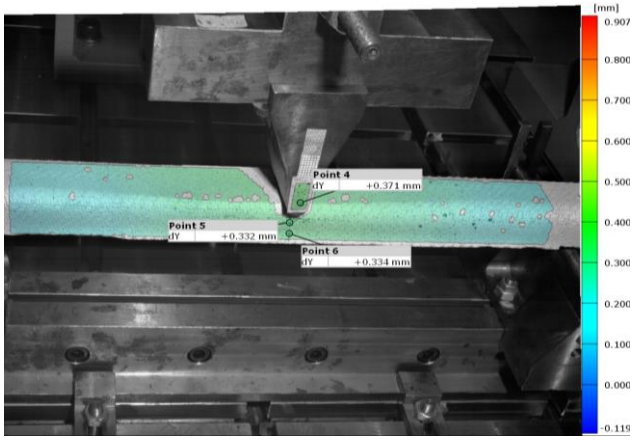

(d) Displacement $v = 0{,}332$ mm for $F = 312{,}41$ N

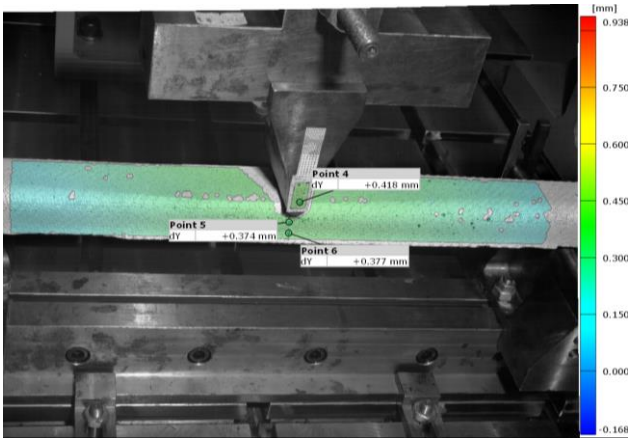

(e) Displacement $v = 0{,}374$ mm for $F = 357{,}64$ N

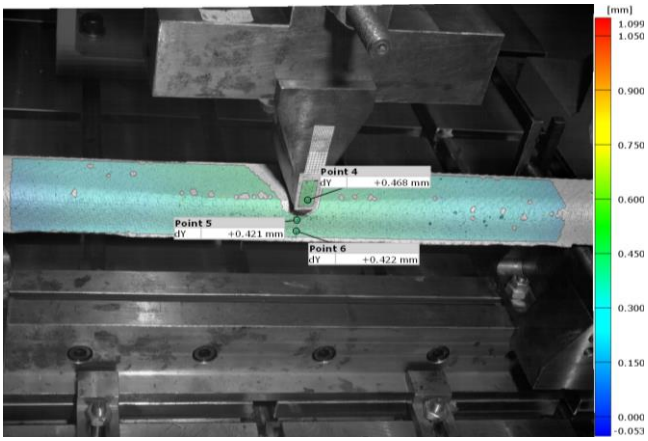

(f) Displacement $v = 0{,}421$ mm for $F = 403{,}38$ N

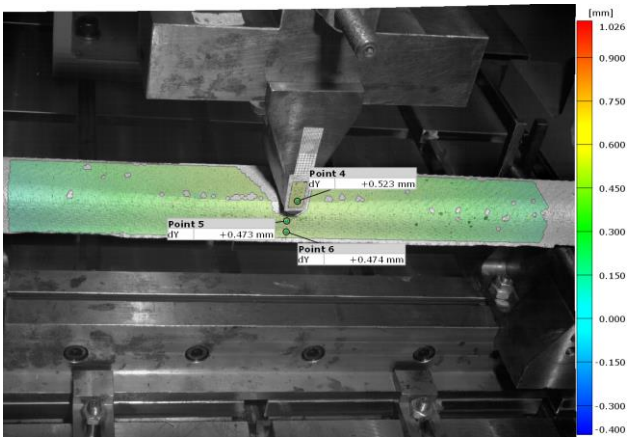

(g) Displacement $v = 0{,}473$ mm for $F = 449{,}51$ N

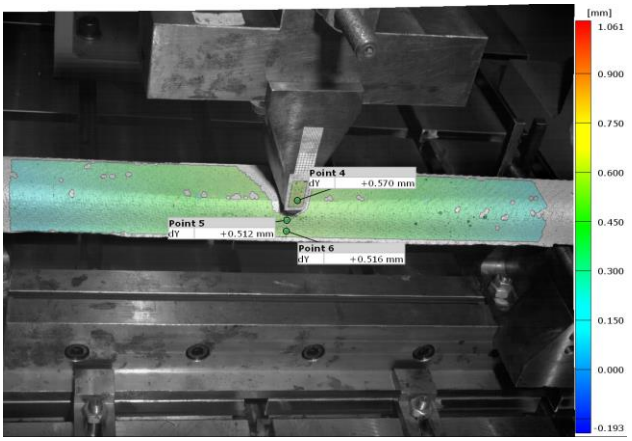

(h) Displacement $v = 0{,}512$ mm for $F = 495{,}41$ N

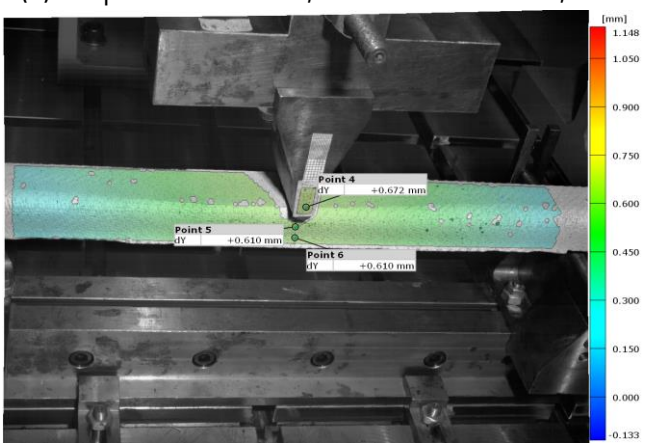

(i) Displacement $v = 0{,}558$ mm for $F = 541{,}57$ N

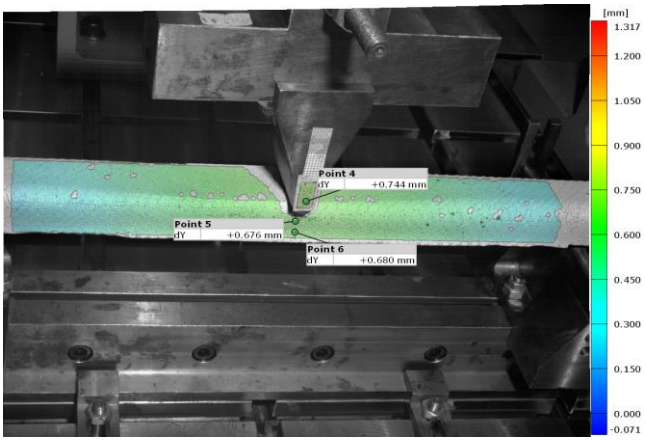

(j) Displacement $v = 0{,}610$ mm for $F = 589{,}21$ N

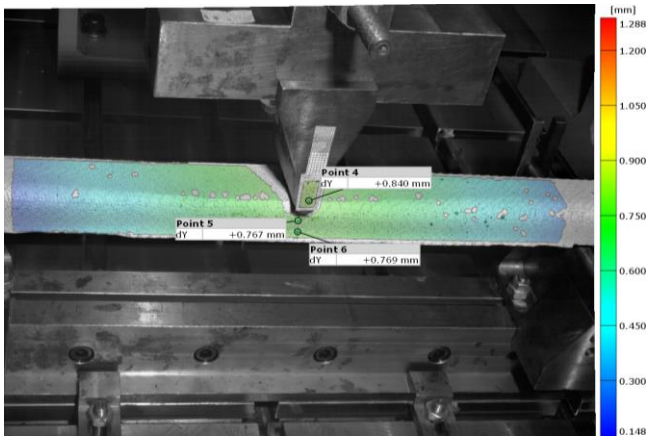

(k) Displacement $v = 0{,}676$ mm for $F = 659{,}01$ N

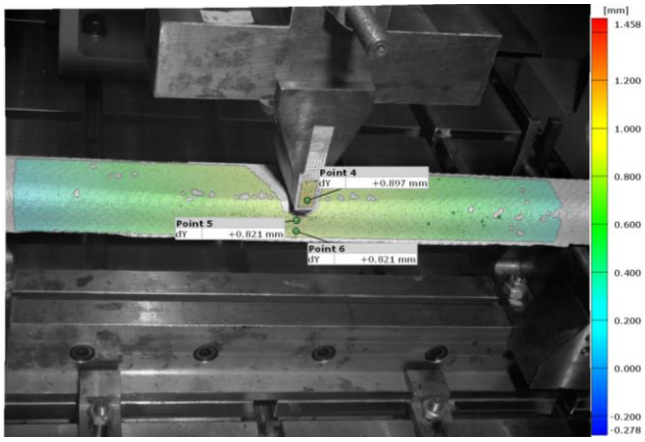

(l) Displacement $v = 0{,}767$ mm for $F = 753{,}86$ N

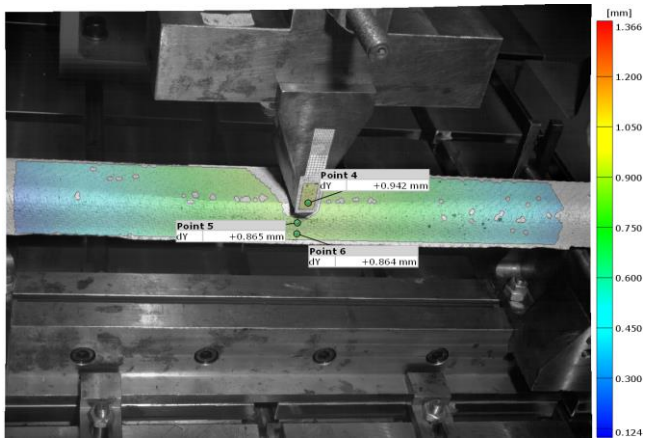

(m) Displacement $v = 0{,}821$ mm for $F = 802{,}31$ N

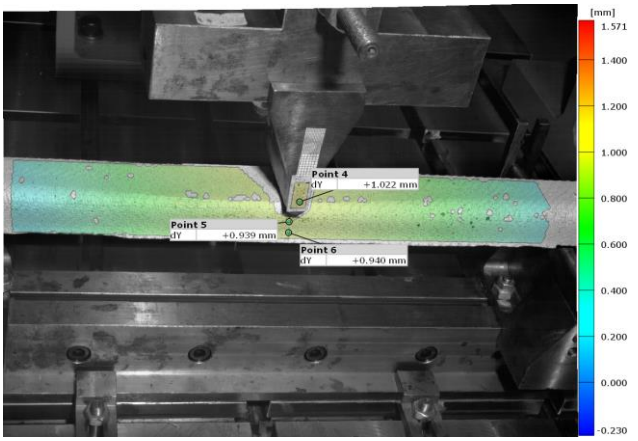

(n) Displacement $v = 0{,}865$ mm for $F = 850{,}69$ N

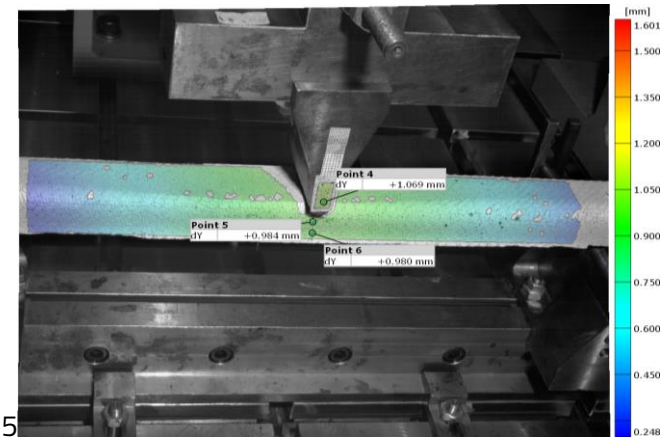

5

(o) Displacement $v = 0{,}939$ mm for $F = 923{,}23$ N

(p) Displacement $v = 0{,}984$ mm for $F = 969{,}90$ N

Figure 7.5. The evolution of the field of displacements in the vertical direction, for the points on the lateral surface of beam 2 made of carbon-aramid/epoxy composite material, located in the area analyzed with the DIC method, depending on the applied force.

After processing the images with the software, the mid-beam deflection versus time curve was obtained, which was then correlated with the force recorded by the test machine using time and the displacement of the point on the load roller. Thus, the force variation curve was obtained as a

function of the vertical displacement at the middle of the beam (curve) by the DIC method for all tested beams (fig. 7.6).

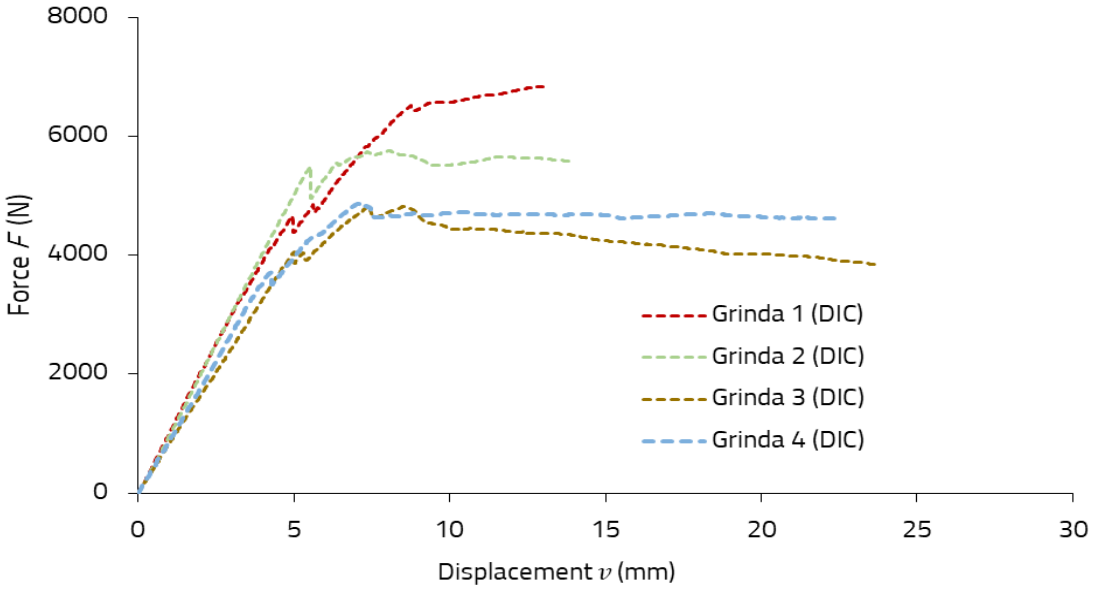

Figure 7.6. Force curve – vertical displacement ($F - v$)for DIC method.

It could be noted that, after the bending test, for none of the tested beams the complete rupture of the eight layers reinforced with carbon-aramid hybrid fabric from their upper part (upper U-profile) was observed, and the lower U-profile (part lower part of the beam) was not affected. No delaminations were found at the interface between the two U-section profiles, which were assembled by gluing.

7.2. Numerical simulation of stress and strain states in the beam made of carbon-aramid/epoxy composite material subjected to bendingmularea numerică a stărilor de tensiune și de deformație din grinda realizată din material compozit carbon-aramidă/ epoxi solicitată la încovoiere

7.2.1. FEA model

In this section, the numerical model will be presented for the thin-walled rectangular section beam (box/rectangular section) made of hybrid composite material, subjected to bending. The numerical simulation of the three-point bending test was carried out using the Abaqus program, version 2022 (Dassault Systèmes, France). The beam made of composite material reinforced with carbon-aramid fabric, for which the mechanical behavior in the bending test was numerically simulated by the three-point method in accordance with the loading scheme in figure 7.2, has the following characteristics:

- the outer dimensions of the cross section are b = 45 mm and h = 35 mm;
- the thickness of the walls is 2.60 mm (8 layers of composite material based on Epolam 2031 epoxy resin, reinforced with carbon-aramid hybrid fabric);

- the total length of the beam is 500 mm;
- the distance between the beam supports is 445 mm.

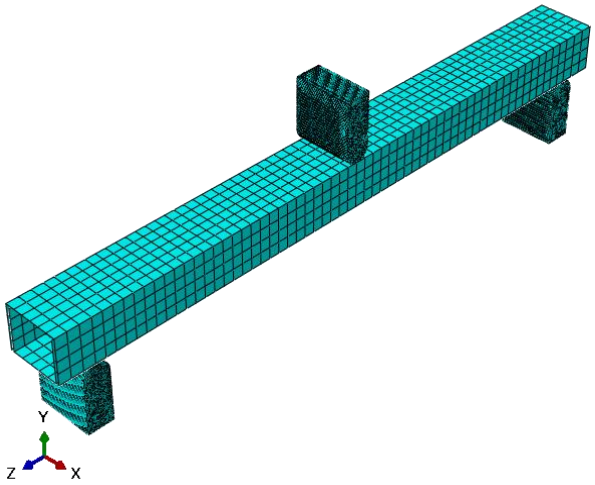

(a)

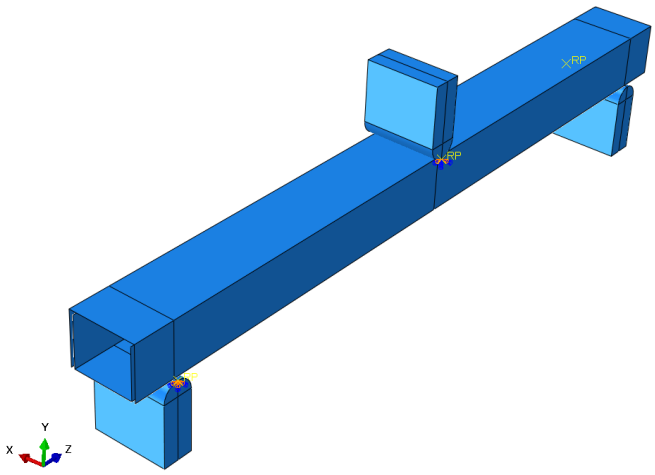

(b)

Figure 7.3. Numerical model: (a) finite element discretization for the beam made of hybrid composite material; (b) imposed boundary conditions.

The elastic properties of the composite material from which the beam was modeled were introduced into the numerical model, considering the experimental results obtained by the author of this thesis, in the bending test of the specimens made of the same composite material as that of the tested beam, which have were also published in another scientific paper [31], namely: the modulus of elasticity = 29343 MPa and = 26884 MPa in the directions of the reinforcing fibers of the carbon-aramid fabric, the Poisson's ratio in the plane of the reinforcement, and the modulus of transverse elasticity MPa in the fabric reinforcement plane, was considered according to the results reported by other authors in the specialized literature [73]. More details regarding the processing of the numerical model of the carbon-aramid/epoxy hybrid composite beam are presented in the doctoral thesis.

7.2.2. Results obtained in finite element analysis

The vertical force-displacement curve at the middle of the beam, obtained after processing the results of the numerical simulation of the beam with rectangular section, with thin walls, made of hybrid composite material, is presented in figure 7.14.

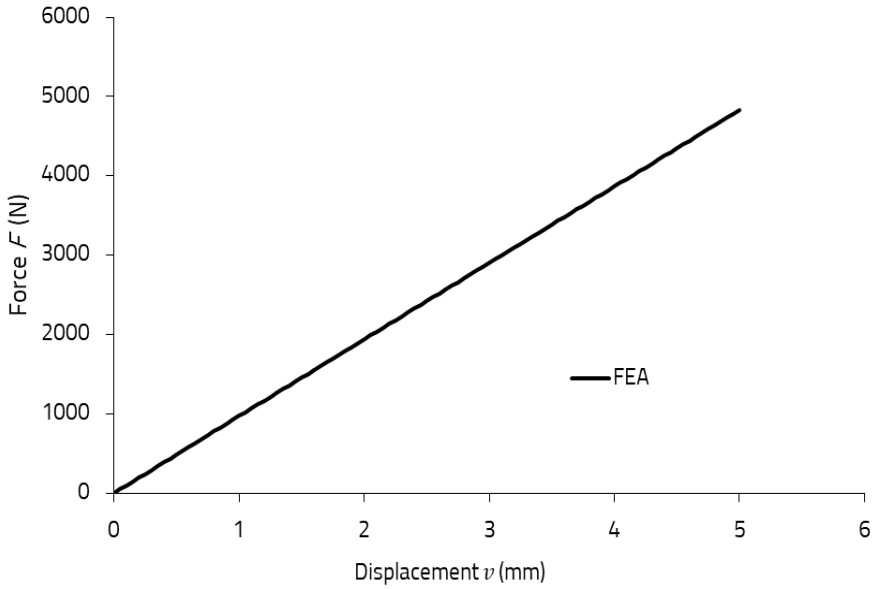

Figure 7.14. Force curve – vertical displacement at the middle of the beam (obtained from numerical simulation ($F - v$).

7.3. Validation of the numerical model by comparing the results obtained by numerical modeling with the experimental ones

Table 7.4 summarizes the data obtained for beam 2, from the point of view of the vertical displacement at the middle of the beam, in a comparative way by the three methods, namely: experimental from the test machine; experimentally by the DIC method; numerical simulation (FEA results). The results are compared for each of the four composite beams tested, for the linear portion of the force-versus-vertical-displacement curve at mid-beam, approximately up to a force of 1000 N. In the doctoral thesis in tables 7.3, 7.5 and 7.6 the data obtained for the other three tested beams (beam 1, beam 3 and beam 4) are presented in a comparative way by the three methods, similar to the data provided in table 7.4.

Table 7.4. Comparative analysis of the results obtained for the v arrow measured in the middle of the beam for beam 2.

	Force Exp.* (N)	Maximum displacement v_{max} (mm)			Error (%)	
		Exp*	DIC	FEA	FEA-DIC	FEA-Exp*
BEAM 2	160,78	0,188	0,172	0,164	4,965	13,163
	203,21	0,241	0,218	0,207	5,257	14,253
	246,17	0,289	0,265	0,250	5,527	13,575
	312,41	0,364	0,332	0,317	4,446	12,957
	357,64	0,414	0,374	0,362	3,009	12,481
	403,38	0,465	0,421	0,408	3,060	12,103
	449,51	0,516	0,473	0,455	3,780	11,810
	495,41	0,565	0,512	0,501	2,146	11,260
	541,57	0,614	0,558	0,548	1,843	10,809
	589,21	0,667	0,610	0,596	2,300	10,580
	659,01	0,739	0,676	0,667	1,326	9,742
	753,86	0,839	0,767	0,763	0,541	9,042
	802,31	0,890	0,821	0,812	1,088	8,770
	850,69	0,940	0,865	0,861	0,400	8,398
	923,23	1,015	0,939	0,935	0,418	7,923
	969,90	1,064	0,984	0,982	0,155	7,681
	1017,81	1,115	1,034	1,031	0,337	7,522

* Exp – stands for the experimental method with the testing machine for the three-point bending test.

Table 7.7 summarizes the average values of the errors calculated for the four composite beams tested.

Table 7.9. Average errors obtained for the experimentally measured maximum displacement v_{max} in the middle (up to 1000 N).

BEAM	Average error (%)	
	FEA-DIC	FEA-Exp*
1	2,98	26,15
2	2,39	10,71
3	15,18	22,77
4	13,09	25,63
Average	8,41	21,31

*Exp – stands for the experimental method with the testing machine for the three-point bending

Explanation of errors related to the maximum arrow

These differences between the maximum deflection results determined experimentally with the test machine and with the digital image correlation (DIC) method are caused by the following factors:

- the displacement recorded with the test machine represents the displacement of the force application punch, and the displacement determined with the DIC method represents the displacement of the marked point on the lateral surface of the beam;
- the upper part of the profile, its material settles and deforms locally in the contact area between the profile and the roll (punch) through which the force is applied;
- on the test machine, the existing clearances in the load force transmission system are cancelled.

7.4. Conclusion

After carrying out the bending tests using the three-point method, for beams made of carbon-aramid/epoxy hybrid composite material, broken layers can be observed only in their upper part, respectively of the upper U-profile, without the lower U-profile of the composite beam be affected. The failure modes of the hybrid composite layers at the top of the beam were: delamination at the fiber-matrix interface, matrix (resin) cracks, and carbon and aramid fiber breakage. It is noted that not all eight carbon-aramid hybrid fabric reinforced layers of the upper part of the beam were broken. The mean value for the maximum sag recorded by the test machine was 20.15 mm, and in the case of the DIC method the mean value for the maximum sag was 18.15 mm, considering the same loading force recorded by the test machine, using time as parameter for data correlation. The finite element analysis of the model for the thin-walled beam made of carbon-aramid/epoxy hybrid composite material was performed under the conditions of an imposed displacement of 5 mm, so that the data processing is done only for the elastic domain. To validate the numerical model, the results obtained from the finite element analysis (FEA) for the maximum displacement at the middle of the beam were compared with the experimental results obtained both with the testing machine and with the DIC method, for bending stress forces of approximately 1000 N.
In this section, only a summary of the conclusions of the doctoral thesis is presented.

8. GENERAL CONCLUSIONS. PERSONAL CONTRIBUTIONS AND FUTURE DIRECTIONS FOR RESEARCHNCLUZII GENERALE. CONTRIBUȚII PERSONALE ȘI DIRECȚII VIITOARE DE CERCETARE

8.1. General conclusion

Taking into account the objectives (see chapter 3) proposed in order to achieve the main goal of this doctoral thesis, we can list the main conclusions of the research carried out in this doctoral thesis:

◘ from the critical analysis of the current state of research on Kevlar fibers, carbon fibers and structures made of hybrid composite materials reinforced with carbon fibers and Kevlar fibers, the following were identified:
- the main advantages of the hybridization of Kevlar fibers (aramid) and carbon fibers can be summed up in obtaining composite materials characterized by: high tensile strength, high rigidity, high impact resistance, low coefficient of thermal expansion and a high modulus of elasticity (see chapter 2.4);
- the main applications regarding the use of composite materials reinforced with carbon fibers and/or Kevlar fibers for strengthening structural elements (wooden or concrete beams, panels) (see chapter 2.3.3);
◘ the elastic and mechanical tensile characteristics of the composite material based on Epolam 2031 epoxy resin, reinforced with carbon-aramid hybrid fabric, were determined using the tensile test combined with the digital image correlation method, namely:
- the longitudinal moduli of elasticity and are equal to: 35242 MPa in the warp direction of the carbon-aramid hybrid fabric and, respectively, to 33626 MPa in the weft direction of the carbon-aramid hybrid fabric (see chapter 5.4.1);
- the maximum normal stresses resulting in relation to the reinforcement directions of the composite material are equal to: 407 MPa in the warp direction of the carbon-aramid hybrid fabric and 372 MPa in the weft direction of the carbon-aramid hybrid fabric (see chapter 5.4.1) ;
- the values of Poisson's coefficients and in the plane of fiber reinforcement, were 0.141 and 0.106, when the tensile force was applied in the warp direction and in the weft direction, respectively, of the carbon-aramid hybrid fabric (see chapter 5.4.1) ;
◘ the elastic and mechanical bending characteristics of the carbon-aramid/epoxy hybrid composite material were determined, namely:
- longitudinal and bending moduli of elasticity: 29343 MPa in the warp direction of the carbon-aramid hybrid fabric and 26884 MPa in the weft direction of the carbon-aramid hybrid fabric (see chapter 5.4.2);
- the resulting maximum normal stresses were: 424 MPa in the warp direction of the carbon-aramid hybrid fabric and 413 MPa in the weft direction of the carbon-aramid hybrid fabric (see chapter 5.4.2);
◘ the validation of the numerical models used to simulate the states of tension and deformation in the specimens made of carbon-aramid/epoxy composite material, which develop in tensile and bending stress respectively, by comparing the results obtained from the numerical analysis with those obtained experimentally (the maximum resulting error was 0.19% for the tensile test and 0.15% respectively for the bending test, see chapter 5.5.2);

◘ the use of analytical models for the calculation of tensile and bending equivalent moduli of elasticity, for the layered composite material of the carbon-aramid/epoxy type, led to results that were validated by the experimental results (see chapter 5.5.1);

◘ the mechanical characteristics regarding impact behavior in the Charpy test were determined for the composite material reinforced with carbon-aramid hybrid fabric, namely:

- the breaking energies obtained are equal to 2.79 J and 2.43 J when the length of the Charpy test piece is parallel to the warp direction and, respectively, to the weft direction, of the carbon-aramid hybrid fabric (see chapter 5.4.3);
- the values obtained for resilience were: 90.49 kJ/m2 and 80.36 kJ/m2 when the length of the Charpy specimen is parallel to the warp direction and, respectively, to the weft direction of the carbon-aramid hybrid fabric (see chapter 5.4.3);
- none of the samples broke completely in the Charpy impact test (see chapter 5.4.3);
- modes of breakage: delaminations between layers, breakage of fibers in some layers, detachment at the fiber-resin interface, as well as cracks in the matrix (see chapter 5.4.3);

◘ from the low-velocity drop impact tests, carried out on specimens of layered composite materials reinforced with carbon-aramid hybrid fabric, with and without a rubber core, tested before immersion in water, the following main conclusions can be noted:

- the replacement by the rubber core of two middle layers in the composite material reinforced only with carbon-aramid hybrid fabric and obtaining the sandwich composite material of the CK2R type, leads to a delay in the energy absorbed during the impact at low velocity, while the impact energy is approximately the same as the absorbed energy;
- from the point of view of the absorbed energy, there is a rather small difference between the two sets of samples, namely, for the impact energy of 25 J, in the case of dry samples of type CK2R the average value of the absorbed energy is only 0,17% lower than that corresponding to dry samples of type CK; for the impact energy of 50 J, dry samples of type CK2R absorbed approximately the same amount of energy as dry samples of type CK (see chapter 6.3.1);
- the maximum displacement recorded for the dry samples of CK2R composite material with a rubber core was approximately 26% and 22% higher than the maximum displacement recorded for the dry samples CK without a rubber core, in the case of impact energies of 25 J and, respectively, of 50 J (see chapter 6.3.1);
- for the impact energy of 25 J, the fracture modes observed are cracks in the matrix and delaminations at the fiber-matrix interface (see chapter 6.3.5);
- for the impact energy of 50 J, breakage of both carbon and aramid fibers was observed in the outer layers of the CK2R composite material with a rubber core, while only breakage of carbon fibers was observed for the CK type composite material, without rubber core (see chapter 6.3.5);

◘ from the analysis of the effects of water absorption on the low-velocity impact behavior of composite materials reinforced with carbon-aramid hybrid fabric, the following main conclusions are drawn:

- for the CK composite material reinforced only with carbon-aramid hybrid fabric, both in the case of those tested at impact before immersion, and in the case of the samples tested after 8440 hours of immersion in water, subjected to an impact energy of 25 J, the amount of absorbed energy is

approximately the same, the difference being only 0.93% compared to the value recorded for dry ones (see chapter 6.3.3 and 6.3.4);
- for the impact energy of 50 J, a significant difference can be observed in terms of the energy absorbed by the CK composite material, as follows: 49.79 J for the dry samples and 41.84 J for the samples tested after 8440 hours of immersion in water, the decrease being 16% (see chapter 6.3.3 and 6.3.4);
- for CK2R samples with a rubber core, both in the case of those tested at impact before immersion, and in the case of samples tested after 10513 hours of immersion in water, subjected to an impact energy of 25 J, the absorbed energy is approximately the same, the difference being only 1.82% compared to the value recorded for dry ones (see chapter 6.3.3 and 6.3.4);
- for the impact energy of 50 J, a significant difference can be observed in the energy absorbed by the CK2R composite material with a rubber core, as follows: 49.77 J for the dry specimens and 26.74 J for the tested specimens, respectively after 10513 hours of immersion in water, the decrease being 53.26% (see chapter 6.3.3 and 6.3.4);
◘ the following results obtained for the thin-walled beam made of carbon-aramid hybrid composite material, using the bending test combined with the digital image correlation method, are mentioned:
- the average value for the maximum deflection recorded by the test machine was 20.15 mm, and in the case of the DIC method the average value for the maximum deflection was 18.15 mm, considering the same load force recorded by the test machine, using the time as a parameter for data correlation (see chapter 7.1.3);
- the validation of the numerical model with finite elements of the beam made of composite material reinforced with hybrid carbon-aramid fabric, subjected to bending, was carried out, by comparison with the obtained experimental results, resulting in an average error of 8.41% for the comparison of the maximum arrow from the FEA with the arrow maximum obtained by the DIC method, and for the comparison of the maximum sag from the FEA with the sag from the experimental method (test machine) an average error of 21.31% resulted, for a force range from 0 N – 1000 N (see chapter 7.3);
- the maximum normal stress in the direction of the fibers resulting from the numerical analysis, does not exceed the breaking stress of 418 MPa, determined in the experimental bending tests on samples made of the same hybrid composite material (see chapter 7.2.2);
- the failure modes of the hybrid composite material layers, at the upper part of the beam, were: delaminations at the fiber-matrix interface, cracks in the matrix (resin) and breakage of carbon and aramid fibers (see chapter 7.1.3);
- it was found that not all the eight layers reinforced with carbon-aramid hybrid fabric of the upper part of the beam were broken and the joint by gluing of the two U-profiles resisted the bending stress, without their peeling (see chapter 7.1.3).

8.2. Personal contributions. Future research directions.

During the research carried out for the preparation of this doctoral thesis, several personal and original contributions were outlined, which are mentioned below.

Theoretical contributions:

- a thorough study was carried out regarding the current state of research related to the mechanical characteristics of carbon fibers and Kevlar (aramid) fibers, which led to the formulation of the main advantages and disadvantages of the hybridization of these two types of fibers (chapter 2) ;
- the importance of using composite materials reinforced with carbon fibers and/or Kevlar (aramid) to strengthen structural elements (concrete beams, wooden beams or sandwich panels) used in civil constructions or in other fields was highlighted (chapter 2);
- the use of analytical calculation models to determine the tensile and bending mechanical characteristics (modulus of elasticity for structures made of hybrid composite material reinforced with carbon fiber and aramid fiber fabric (chapter 4 and chapter 5);
- the numerical simulation of the mechanical tensile and bending stresses was carried out, for the analysis of the stress and deformation states that develop in the structures made of hybrid composite material reinforced with carbon-aramid fabric, and the obtained results were validated by the experimental results (chapter 5);
- the numerical model of the beam made of composite material, reinforced with carbon-aramid fabric, having a rectangular section, with thin walls, formed by joining two U-profiles, was made, considering the elastic properties determined in the doctoral thesis, for modeling the material (chapter 7) .

Experimental contributions:

- the manufacture by manual forming technology of plates made of hybrid composite material reinforced with carbon-aramid fabric, from which the necessary specimens were cut for the tensile, bending, impact tests by the Charpy test and low-velocity impact (chapter 5);
- the design and manufacture of metal molds (U-type profiles), necessary for the manufacture of beams from hybrid composite material reinforced with carbon-aramid fabric (chapter 7);
- the manufacture by manual layering technology of beams from layered composite material, reinforced with hybrid aramid-carbon fabric, which were subjected to the bending test combined with the digital image correlation method (chapter 7);
- determination of the elastic and resistance characteristics through the tensile test which was carried out simultaneously using both the test machine and the optical method of measuring deformations through the digital correlation of images (chapter 5);
- the determination of the following mechanical and elastic characteristics for the samples made of carbon-aramid hybrid composite material, studied in this scientific work: longitudinal tensile modulus (Young's modulus), longitudinal flexural modulus,

tensile strength, tension maximum normal bending, resilience in impact stress by the Charpy test (chapter 5);

- determining the values of Poisson's ratio (transverse contraction coefficient) in the reinforcement plane, for the composite material reinforced with carbon-aramid fabric, using the digital image correlation method (chapter 5);
- processing absorption data during immersion in water and determining with Fick's law, the water diffusion coefficient in the hybrid composite material reinforced with carbon-aramid fabric (chapter 6);
- the comparative analysis regarding the behavior in low-velocity impact stress (absorbed energy, failure modes), of the composite material reinforced only with carbon-aramid hybrid fabric and of the sandwich composite material, with faces reinforced with the same carbon-aramid fabric and with a rubber core (Chapter 6);
- the study of the influence of humidity on the behavior in low-velocity impact stress (absorbed energy, displacement, force, failure modes), of structures made of composite materials reinforced with carbon-aramid hybrid fabric, with and without a rubber core (chapter 6);
- the use of the digital image correlation method (DIC method) for the experimental analysis of the distribution of displacements in the case of beams made of composite material reinforced with hybrid aramid-carbon fabric, subjected to bending (chapter 7);
- experimental determination of the maximum deflection for composite beams reinforced with aramid-carbon hybrid fabric, using the testing machine and using the results for additional validation of the numerical model of the beam, in addition to validation with the results obtained with the optical method of measuring deformations by the method 3D image correlation optics (Chapter 7).

REFERENCES

1. **Ursache, S.**, Cerbu, C., Hadăr, A., *Characteristics of Carbon and Kevlar Fibres, Their Composites and Structural Applications in Civil Engineering - A Review*. Polymers, 2024. **16**(1).
2. Jassal, M. and S. Ghosh, *Aramid fibres - An overview.* Indian Journal of Fibre & Textile Research, 2002. **27**(3): p. 290-306.
3. Manigandan, S., et al., *Numerical investigation of low velocity out of plane impact behavior of Kevlar composites.* Materials Today-Proceedings, 2019. **16**: p. 994-998.
4. Potluri, R., K.J. Paul, and B.M. Babu, *Effect of Silicon Carbide Particles Embedmenton the properties of Kevlar Fiber Reinforced Polymer Composites.* Materials Today-Proceedings, 2018. **5**(2): p. 6098-6108.
5. Kevlar Aramid Fiber Technical Guide. Available online: https://www.dupont.com/content/dam/dupont/amer/us/en/safety/public/documents/en/Kevlar_Technical_Guide_0319.pdf
6. Li, X.G. and Huang, M.R., *Thermal degradation of Kevlar fiber by high-resolution thermogravimetry.* Journal of Applied Polymer Science, 1999. **71**(4): p. 565-571.
7. Liu, X.Y. and Yu, W.D., *Evaluating the thermal stability of high performance fibers by TGA.* Journal of Applied Polymer Science, 2006. **99**(3): p. 937-944.
8. Rojstaczer, S., Cohn, D., and Marom, G., *Thermal-Expansion Of Kevlar Fibers And Composites.* Journal of Materials Science Letters, 1985. **4**(10): p. 1233-1236.
9. Dixit, P., Ghosh, A., and Majumdar, A., *Hybrid approach for augmenting the impact resistance of p-aramid fabrics: grafting of ZnO nanorods and impregnation of shear thickening fluid.* Journal of Materials Science, 2019. **54**(20): p. 13106-13117.
10. Minoshima, K., Tsuru, K., and Komai, K., *Influence of vacuum and water on tensile fracture behaviour of aramid fibres.* Damage and Fracture Mechanics: Computer Aided Assessment and Control, Southampton, UK,1998. p. 595-604.
11. Ertekin, M., *Fiber Technology for Fiber-Reinforced Composites*. Woodhead Publishing, Sawston, UK, 2017. p. 153-167.
12. Krucinska, I. and Stypka, T., *Direct measurement of the axial Poisson ratio of single carbon-fibers.* Composites Science and Technology, 1991. **41**(1): p. 1-12.
13. Bhatt, P. and A. Goel, *Carbon Fibers: Production, Properties and Potential Use.* Material Science Research India, 2017. **14**(1): p. 52-57.
14. Newcomb, B.A., *Processing, structure, and properties of carbon fibers.* Composites part a-applied science and manufacturing, 2016. **91**: p. 262-282.
15. Goodhew, P.J., Clarke, A.J., and Bailey, J.E., *A Review of the Fabrication and Properties of Carbon Fibres.* Materials Science and Engineering, 1975. **17**(1): p. 3-30.
16. Huang, X.S., *Fabrication and Properties of Carbon Fibers.* Materials, 2009. **2**: p. 2369-2403.
17. Ou, R.X., et al., *Reinforcing effects of Kevlar fiber on the mechanical properties of wood-flour/high-density-polyethylene composites.* Composites Part A-Applied Science and Manufacturing, 2010. **41**: p. 1272-1278.
18. Alam, P., Mamalis, D., Robert, C., Floreani, C., Brádaigh, C.M.O., *The fatigue of carbon fibre reinforced plastics—A review.* Compos, Part B Eng, 2019. **166:** p. 555–579.
19. Dieter, L., et al., *Poisson Ratio Carbon Fibers At The Microscopic and the Nanoscopic Scale*. In Proceedings of the Carbon Conference, Providence, RI, USA, 11-16 July, 2004.

20. Zollner, M., et al., *Thermal resistance of carbon fibres/carbon fibre reinforced polymers under stationary atmospheric conditions and varying exposure times.* Waste Management, 2019. **85**: p. 327-332.
21. Chung, D.D.L., *Carbon fiber composites*. Butterworth-Heinemann, Oxford, UK, 1994. p. 65-78.
22. Xiao, H., Lu, Y., Zhao, W., and Qin, X., *The effect of heat treatment temperature and time on the microstructure and mechanical properties of PAN-based carbon fibers*. J. Mater. Sci, 2014. **49**: p. 794–804.
23. Pradere, C. and C. Sauder, *Transverse and longitudinal coefficient of thermal expansion of carbon fibers at high temperatures (300-2500 K).* Carbon, 2008. **46**(14): p. 1874-1884.
24. Tye, L., *The tensile behavior of high-strength carbon fibers.* Microscopy and Microanalysis, 2016. **22**(4): p. 841-844.
25. Emmerich, F.G., *Young's modulus, thermal conductivity, electrical resistivity and coefficient of thermal expansion of mesophase pitch-based carbon fibers.* Carbon, 2014. **79**: p. 274-293.
26. Zhang, Z.H., et al., *Carbon Fibers with High Electrical Conductivity: Laser Irradiation of Mesophase Pitch Filaments Obtains High Graphitization Degree.* Acs Sustainable Chemistry & Engineering, 2020. **8**(48): p. 17629-17638.
27. Gupta, A., et al., *Effect of graphitization temperature on structure and electrical conductivity of poly-acrylonitrile based carbon fibers.* Diamond and Related Materials, 2017. **78**: p. 31-38.
28. Sanjay, M.R., Arpitha, G.R., and B. Yogesha, B., *Study on Mechanical Properties of Natural - Glass Fibre Reinforced Polymer Hybrid Composites: A Review.* Materials Today-Proceedings, 2015. **2**(4-5): p. 2959-2967.
29. Xu, D.H., et al., *Analysis of the hybrid composite materials reinforced with natural fibers considering digital image correlation (DIC) measurements.* Mechanics of Materials, 2019. **135**: p. 46-56.
30. Dorey, G., Sidey, G.R., and Hutchings, J., *Impact properties of carbon fibre/Kevlar 49 fibre hybrid composites.* Composites, 1978. **9**: p. 25-32.
31. Cerbu, C., **Ursache, S.,** Botis, M.F., Hadăr, A. *Simulation of the Hybrid Carbon-Aramid Composite Materials Based on Mechanical Characterization by Digital Image Correlation Method.* Polymers, 2021. **13**(23).
32. **Ursache, S.**, Cerbu, C., Hadăr, A., Dumbrava, F., *Aspects regarding the mechanical charateristics of the carbon-Kevlar composite materials*. In Procedings of The 9th International Conference on Advanced Composite Materials Engineering (COMAT), Brasov, 17 – 18 October, 2022.
33. Haidzir, H., et al., *Modal Properties of Hybrid Carbon/Kevlar Composite Thin Plate and Hollow Wing Model* Applied Mechanics and Materials Vols. 446-447 (2014) pp 597-601, 2013.
34. Karthik, K., et al., *Experimental investigation on the mechanical properties of Carbon/Kevlar fibre reinforced epoxy LY556 composites.* Materials today: Proceedings, 2021. **52**: p. 668-674.
35. Jang, B.Z., et al., *Impact Resistance And Energy-Absorption Mechanisms In Hybrid Composites.* Composites Science and Technology, 1989. **34**(4): p. 305-335.
36. Gustin, J., et al., *Low velocity impact of combination Kevlar/carbon fiber sandwich composites.* Composite Structures, 2005. **69**(4): p. 396-406.
37. Han, Y., Liu, H.B., and Guo. T., *Analysis of Bending Stiffness of Reinforced Concrete Beams Strengthened with Carbon Fiber Sheet*. International Conference on Civil, Architectural and Hydraulic Engineering (ICCAHE 2012), Zhangjiajie, China, 2012. p. 2887-2890.
38. Takeda, K., et al., *Flexural behaviour of reinforced concrete beams strengthened with carbon fibre sheets.* Composites Part a-Applied Science and Manufacturing, 1996. **27**(10): p. 981-987.

39. Chen, D., Y.D. Liao, and Y. Zhang, *Experimental Study of RC Beams Strengthened with Basalt Fiber Sheets.* Chinese-German Joint Symposium on Hydraulic and Ocean Engineering (Cg Joint 2010), 2010: p. 463-466.
40. Garcia, P.D., Escamilla, A.C., and Garcia, M.N.G., *Bending reinforcement of timber beams with composite carbon fiber and basalt fiber materials.* Composites, 2013. **55**: p. 528-536.
41. Shekarchi, M., Oskouei, A.V., and Raftery, G.M., *Flexural behavior of timber beams strengthened with pultruded glass fiber reinforced polymer profiles.* Composite Structures, 2020. **241**.
42. Sitorus, T., and S. Desharma. S., *Analysis and experiments of the effect of reinforcement of wood beam using carbon fiber reinforced polymer against bending strength*. 4th International Conference on Sustainable Civil Engineering Structures and Construction Materials (SCESCM), Yogyakarta, INDONESIA, 2018.
43. Zweben, C., *Flexural strength of aramid fiber composites.* Journal of Composite Materials, 1978. **12**(OCT): p. 422-430.
44. Singh, T.J., and S. Samanta, S., *Characterization of Kevlar Fiber and Its Composites: A Review.* Materials Today-Proceedings, 2015. **2**(4-5): p. 1381-1387.
45. Pandulu, G., Jayaseelan, R., and Jeganathan, S., *Performance of RCC Beams Laminated with Kevlar Fabric.* Jordan Journal of Civil Engineering, 2020. **14**(2): p. 225-237.
46. Tang, T.P., and Saadatmanesh, H., *Behavior of concrete beams strengthened with fiber-reinforced polymer laminates under impact loading.* Journal of Composites for Construction, 2003. **7**(3): p. 209-218.
47. Liu, W., et al., *Impact resistance of CFRP-reinforced wood beams under axial force using a digital image correlation method.* Composite Structures, 2021. **261**.
48. Cerbu, C., *Materialele compozite şi mediul agresiv. Aplicații speciale*. 2006, Editura Universitatii Transilvania Brasov, Brasov.
49. Hadăr, A., *Structuri din compozite stratificate - Metode, algoritmi şi programe de calcul*. 2002, Editura Academiei Romane, București.
50. Ever, J. Barbero., *Introduction to composite materials design*. 1998, CRC Publisher, USA. ISBN 978-1-138-19680-3.
51. Cerbu, C., and Curtu, I., *Mecanica şi rezistența materialelor compozite*. 2009, Editura Universitatii Transilvania Brasov, Brasov.
52. Biț, C.S., Curtu, I., Crișan, R., *Rezistența materialelor şi teoria elasticității: curs şi aplicații, partea II -a*. 1998, Editura Universitatii Transilvania Brasov, Brasov.
53. Năstăsescu V., Bârsan Gh., *Elasticitate și Plasticitate : capitole speciale.* 2021, Editura Academiei Forțelor Terestre "Nicolae Bălcescu", Sibiu. ISBN 978-973-153-429-9.
54. Ciofoaia, V., ş.a. *Metoda elementelor finite*. 2001, Editura Infomarket, Braşov. ISBN 973-8204-11-9.
55. Vlase, S., Teodorescu, H., Goia, I., Modrea, A., Scutaru, L., *Materiale compozite. Metode de calcul*. 2007, Editura Universitatii Transilvania Brasov, Brasov. ISBN 978-973-635-890-6.
56. Scutaru, L., Chiru, A., Vlase, S., Cofaru, C., Teodorescu, H., *Materiale plastice si compozite in ingineria autovehciulelor.* 2013, Editura Matrixrom, Bucuresti. ISBN 978-606-250-023-8.
57. Jiga, G. GH., *Noțiuni fundamentale în mecanica materialelor compozite.* 2004, Editura Atlas Press SRL, București. ISBN 973-7767-00-4.
58. Sorohan, S., Sandu, M., Sandu, A., Constantinescu, D.M., *Finite Element Models Used to Determine the Equivalent In-Plane Properties of Honeycombs.* Materials Today Proceedings, 2016. **3**(4): p. 1161-1166.
59. *Fisa tehnica - Țesătură SIGRATEX H W215-TW 2/2.*

60. **Ursache, S.,** Cerbu, C., Hadăr, A., Petrescu, H.A., *Effects of rubber core on the Mechanical Behaviour of the Carbon-Aramid Composite Materials Subjected Low-Velocity Impact Loading Considering Water Absorption*. Articol înregistrat la revista Materials, care este în procedura de recenzie.
61. *Fisa tehnica - Rășină epoxidică EPOLAM 2031.*
62. *SR EN ISO 527-4:2000 - Materiale Plastice. Determinarea proprietăților de tracțiune.*
63. *ISO 179-1:2000 - Materiale plastice. Determinarea caracteristicilor la şoc Charpy.*
64. *SR EN ISO 14125:2000 - Compozite de materiale plastice armate cu fibre. Determinarea proprietăților de încovoiere.*
65. Gilles, M., *Aramid Fibre.* Available online: https://www.final-materials.com/gb/21-aramid-fibre (accessed on 28.06.2024).
66. *Fisa tehnica - Placă tehnică din cauciuc de uz general economică.*
67. *Fisa tehnica - Adeziv epoxidic bicomponent BIZON.*
68. EN ISO 6603-2:2000 - Materiale plastice. Determinarea comportării la şoc prin perforare a materialelor plastice rigide. Partea 2: Încercarea la şoc instrumental.
69. EN ISO 7765-2:2022 - Plastic film and sheeting. Determination of impact resistance by the free -falling dart method - Part 2: Instrumented puncture test.
70. SR EN ISO 62:2008 - Materiale Plastice. Determinarea absorbției de apă.
71. Cerbu, C., and Cosereanu, C., *Moisture Effects on the Mechanical Behavior of Fir Wood Flour/Glass Reinforced Epoxy Composite.* BIORESOURCES, 2016. **11**(4): p. 8364-8385.
72. Naceri, A., *An analysis of moisture diffusion according to Fick's law and the tensile mechanical behavior of a glass-fabric-reinforced composite.* Mechanics Of Composite Materials, 2009. **45**(3): p. 331-336.
73. Coutu; D., V., B., P., T., C., F, *Experimental validation of the 3D numerical model for an adaptive laminar wing with flexible extrados.* In Proceedings of the The 18th International Conference of Adaptive Structures and Technologies, 3-5 October, 2007, Ottawa, Ontario, Canada.